R. & M. No. 3288

MINISTRY OF AVIATION

AERONAUTICAL RESEARCH COUNCIL
REPORTS AND MEMORANDA

Experiments on a Delta Wing with Jet-Assisted Lift

By W. H. MELBOURNE, B.E.

LONDON: HER MAJESTY'S STATIONERY OFFICE
1962
PRICE: 18*s.* 6*d.* NET

Experiments on a Delta Wing with Jet-Assisted Lift

By W. H. Melbourne, B.E.

*Reports and Memoranda No. 3288**

May, 1960

Summary. This report describes an investigation into the effect of blowing a jet stream, simulating conventional jet engines, downwards from the lower surface of a slender delta wing (aspect ratio unity), for the purpose of obtaining additional lift at take-off and landing. Initial experiments investigated a spanwise jet sheet blown respectively from 70, 80 and 90 per cent of the mid-chord from the apex, and a trailing-edge jet flap. It was found that a spanwise jet blown forward of the trailing edge was inefficient in providing lift; a flow investigation showed that this was associated with a region of low pressure behind the jet and a strong vortex at the outer edge of the jet.

Further experiments were then carried out using a narrow chordwise jet sheet and a concentrated group of jets on the wing centre-line, to avoid the adverse effects of the spanwise jet. The concentrated jets proved far more efficient than the other two arrangements, and a total recovery of the thrust component and up to 75 per cent recovery of the lift component of the jet reaction (for the jet directed at 60 deg to the wing plane) was achieved. Tests with the concentrated jets were also made with ground effect and elevator control. The experiments indicated that it does not seem possible to realise more than 90 per cent of the lift component of the jet reaction from any suitably located jet.

1. *Introduction.* For the past decade there has been an increasing interest in research into the possible advantages of blowing and sucking various jet streams from aircraft wings and ducts. These have included boundary-layer control, blowing over flaps, the jet flap and vertical take-off aircraft using pure jet reaction. The first two have been used successfully on production aircraft, while the latter two are still in an experimental stage. One of the future applications of jet blowing is on the very slender supersonic transport aircraft, which has such a bad low-speed performance that considerable thought has been given to methods of increasing the lift at take-off and landing speeds.

In 1957 a programme of wind-tunnel research was commenced at the Imperial College to investigate the effects of blowing a jet stream from the lower surface of a slender delta wing of aspect ratio unity. The model parameters were derived from the current trend of supersonic research at the Royal Aircraft Establishment, at Farnborough and Bedford. There had been no known previous

* Previously issued as Imperial College of Science and Technology, Aeronautics Department Report No. 101—A.R.C. 21,968 (with revision July, 1961).

work on blowing a jet stream from a slender delta wing except a brief investigation at the R.A.E. into blowing laterally from the leading edge. Hence the present research was necessarily of an exploratory nature.

A certain amount of knowledge was drawn from the experiences of Anscombe and Williams[1] for the development of the half-model jet-blowing rig, and the flexible coupling, air-bearing is a development of their flexible coupling. Because of the slender planform adopted it was necessary to eliminate almost entirely any interference of the half-model reflection plane. This was accomplished successfully by boundary-layer control and as this aspect of half-model testing has received little attention there is a section discussing the problem and suggesting further improvements.

The material in this report formed part of a University of London Ph.D. Thesis[14], and the complete thesis included a section on stability using the time-vector method[2], and some performance estimates.

2. *Wind-Tunnel Model.* 2.1. *Model Parameters.* The model was designed in 1957 with the knowledge of current research being carried out on slender delta wings. An aspect ratio of one was chosen (76 deg sweepback), and although for low-speed testing the exact thickness distribution is not very important, a new approach was investigated.

At this time measurement of drag at zero lift being conducted at Bedford favoured an area distribution known as the Lord V for reasons based on drag calculations using the linearised slender-body theory[3,4]. These models had a diamond cross-section, being one of the simplest sections for which the linearised, slender-body, potential equation can be solved. However, from a practical point of view these diamond cross-sections produce very thin tip sections, and for this reason it was decided, for the jet-blowing model, to derive the co-ordinates of an uncambered constant thickness/chord ratio delta wing, having a Lord V area distribution. The derivation of the equation of the centre section is given in Appendix I.

This equation produces a wing with a rounded leading edge and the interesting feature that the centre section from $x = 0{\cdot}4$ to the trailing edge is nearly flat (x, y, z are non-dimensional Cartesian co-ordinates based on the wing centre-line chord c_0, with the origin at the apex, x lying along the wing centre-line chord, and z normal to the chordal plane of the wing). The surfaces of the model wing were therefore made flat over the rear part, thus simplifying the construction and interchangeability of the jet units. The extra thickness thereby provided near the trailing edge helped to make the model sufficiently rigid to withstand the internal pressure. The non-dimensional volume (ν) of the wing was chosen at $0{\cdot}00563$ to conform with the Lord V wing of aspect ratio unity being tested at Bedford. The thickness/chord ratio of the wing is 6 per cent.

2.2. *Jet-Blowing Parameters and the Tunnel-Testing Reynolds Number of the Model.* The following are the parameters used to define the jet-blowing characteristics, and the range of values for which the model tests were conducted.

Jet momentum coefficient, C_μ, $0{\cdot}25$ to $5{\cdot}0$.

Jet velocity ratio, v_J/V_0, 6 to 30.

Jet area ratio, S_J/S, $0{\cdot}18$ per cent to $0{\cdot}71$ per cent.

Jet angle to the wing chordal plane, α_J, 30, 60 and 90 deg,

where

C_μ Jet momentum coefficient $= \dfrac{(m_J/g)v_J}{\frac{1}{2}\rho V_0^2 S}$

v_J Theoretical jet velocity (ft/sec) reached on isentropic expansion from the stagnation pressure p_D in the wing plenum chamber to free-stream pressure p_0

V_0 Free-stream velocity (ft/sec)

S_J Jet exit area (ft^2)

S Wing area (ft^2)

m_J Measured mass flow of the jet (lb/sec)

g Acceleration due to gravity (32·2 ft/sec^2)

ρ_0 Free-stream density (slugs/ft^3).

The range of values for the jet area ratio is low in comparison with the current trends: this is discussed in Section 6.1.

The model was tested in the wind tunnel at a Reynolds number of $5{\cdot}20 \times 10^5$ and $8{\cdot}35 \times 10^5$, based on the aerodynamic mean chord. The approximate tunnel speeds for these two Reynolds numbers are respectively 50 ft/sec and 80 ft/sec.

Fig. 1 shows the co-ordinate system used and the nomenclature to define the jet position, shape and size.

2.3. *Model Construction.* A half-model technique was selected. The model (Fig. 5) was made basically in two sections. The hollow rear plenum chamber of which the wing profile was made up of two flat plates to which the various jet units were attached externally, the two plates being supported by a root-chord member and a main spar running from 0·3 of the root chord to the tip. A laminated mahogany section made up the leading-edge profile forward of the main spar. The high-pressure air was admitted to the plenum chamber centrally through the main structural root-chord member, which was also used as the anchoring member to the model-support ducting, which was in turn supported on the balance.

The root chord (c_0) of the model is 30 in. and the semi-span (s) is 7·5 in. Static-pressure tappings were made at 36 points on the upper and lower surfaces of the wing.

3. *Wind-Tunnel Test Rig.* It was decided to mount the model through a false tunnel wall instead of using the tunnel wall as the reflection plane in order to place the model nearer the centre of the tunnel and to reduce the asymmetric loads applied to the centrally-located overhead balance, and also to reduce the boundary-layer thickness.

Figs. 2 and 3 show the layout of the model-support system in the wind tunnel. The compressed air was supplied through a constant-pressure valve at any pressure up to 100 p.s.i. From this supply the actual flow of air to the model is controlled by a gate-type valve, and the mass flow is measured using an orifice plate[5].

The half model is attached to a section of the air ducting which is supported by struts from the three-component balance. The attachment between the half model and the model-support ducting is made through a clearance hole in the false wall. Initially the problem of transferring the air into

the model-support ducting with a minimum of restraint to the balance movement and zeros was partially overcome by using a very thin rubberised-canvas, flexible connecting tube (or coupling); similar to that used at the R.A.E.[1] However, during the initial tests it was found possible to eliminate entirely balance-constraint corrections, and to almost eliminate the balance-zero corrections (caused by uneven flexure of the coupling under pressure) by removing the jubilee clips securing the flexible coupling to the earthed supply ducting. As shown in Fig. 7 this modification effectively means that one end of the flexible coupling is floating on an air-bearing and is free to distort unevenly without transferring the load through to the balance system.

3.1. *Model Support and Associated Aerodynamic Problems.* The basic problem involved with the half-model technique is that of representing a mirror-type image in the flow pattern of the other half of the wing. This mirror image is obtained by the use of a reflection plane, the false wall, shown in Fig. 4. To obtain the ideal image, the false wall should, (1) have no boundary layer, (2) have a sealed joint on the model centre-line, and (3) be sufficiently large to eliminate three-dimensional end effects. This aim is not fully achieved in practice.

The false wall was made very large in comparison with the model, going entirely from the tunnel floor to the roof and extending $\frac{2}{3}c_0$ in front of the model and c_0 behind. Fig. 3 shows a sketch of the mechanical means by which the model and model-support ducting are mounted on the three-component balance; and also the way in which the flexible coupling, air-bearing is connected. The model is attached asymmetrically (1·9 in. off centre) to a 12 in. diameter circular disk, the centre of which is lined up with the balance-strut attachment points on top of the model-support ducting. This was done to avoid the more complicated system of having to put the balance-strut attachment points in the middle of the ducting. The circular disk is set flush with the surface of the false wall with a 0·030 in. clearance around the edge, to allow for balance movement and part of the boundary-layer control. A gap of $\frac{1}{16}$ in. was left between the model and the circular disk, and to reduce flow through this gap, a thin felt strip was glued to the model.

The error due to the drag of the circular disk and the tail strut is very small, but a calibration was carried out and the appropriate correction made to all the balance readings.

3.2. *The Boundary Layer on the False Tunnel Wall and Flow in the Working Section.* As with all half-model techniques, the problem of producing as near the ideal reflection plane as possible causes some difficulty. The semi-span of the present model is only 7·5 in. and it was decided that velocity in the boundary layer near the model should not be less than 99 per cent of the free-stream value at a distance of 0·10 in. from the false wall. This was achieved by sucking away the boundary layer through a series of perforations.

The false wall is fitted with a rounded leading edge and an 11 per cent full-span trailing-edge flap. Without the flap, the boundary layer was turbulent following a separation bubble at the leading edge. This was due to the strong circulation around the false wall caused by the blockage of the model-support ducting fairing at the back. With the flap adjusted to compensate for the blockage (*i.e.*, produce the condition of no circulation around the false tunnel wall), the boundary layer was laminar to a distance of approximately 10 in. from the leading edge. The flap angle was then increased farther to 30 deg to produce a slightly lower pressure on the back of the false wall than on the front. This increase had no adverse effects on the flow and the pressure differential was used to bleed the boundary layer through perforations in the false tunnel wall from the front to the back.

Fig. 8 shows the overall stages of improvement of the boundary-layer thickness on the false wall and Figs. 9 and 10 show the final boundary-layer thickness and static-pressure variation over the wall next to the model.

At the first row of perforations, mechanical suction was applied.

The boundary-layer measurements were made with small static and total-head tubes mounted on a traverse gear which could be operated from outside the tunnel for any given position on the false tunnel wall. The measurements and adjustments of the boundary layer were carried out at 50 ft/sec and also checked at 80 ft/sec (Fig. 9).

Fig. 11 shows the velocity distribution measured by a pitot-static traverse in a plane at the apex of the model. This shows that the flow was quite satisfactory, the maximum deviation at 50 ft/sec being $\pm$ 0·5 per cent.

3.3. *Air Supply.* The air supply for the jet, which is tapped from the high-pressure storage bottles, varies in pressure between 400 p.s.i. and 1000 p.s.i. The high-pressure supply pipe finishes with a stop valve about 15 ft from the 5 ft $\times$ 4 ft wind-tunnel working section (Fig. 2). A Hale Hamilton pressure controller is connected to the high-pressure supply just after the stop valve. This arrangement provided the air supply to a reservoir at any pre-determined pressure up to 50 p.s.i. which was needed to carry out the tests.

The flow to the model jet is controlled by the main control valve at the end of the reservoir pipe. The mass flow is measured by an orifice plate[5]. The pressure difference across the orifice in inches of water, and the pressure at the upstream tapping in inches of mercury are measured and shown on the main control panel. One other measurement which is shown on the main control panel is the stagnation pressure inside the model plenum chamber. These last three pressure measurements mentioned are necessary to calculate the mass flow and velocity of the jet, which determine the non-dimensional jet momentum coefficient.

3.4. *Flexible Coupling, Air-Bearing Connector.* This connector is used to transfer the high-pressure air into the model suspended on the balance system with a minimum of interference to the balance measurement. The side of the air supply which is attached to the floor is referred to as the earthed supply ducting.

Basically the system is similar to the flexible rubberised-canvas coupling developed at the R.A.E.[1] The end of the flexible coupling, which is normally fixed to the earthed supply ducting, is disconnected and allowed to float freely on an air-bearing. The air for the air-bearing is conveniently bled from the main supply and this air loss is kept relatively small and accurately calibrated.

The general layout of the model with respect to the connector and the earthed supply ducting is shown in Fig. 3 and Fig. 6 is a photograph of the connector in position. The model is supported asymmetrically and hence the earthed supply ducting is rotated in the same manner as the model incidence by a leadscrew device. Fig. 7 is a detailed drawing of the connector which is $3\frac{1}{2}$ in. diameter by 12 in. long and is constructed of four layers of $\frac{1}{64}$ in. thick rubberised-canvas sheeting, reinforced with four extra layers at each end. The end of the flexible coupling attached to the model-support ducting was made a tight fit, and then the jubilee clips were tightened up with the coupling pressurised to avoid initial distortion of the rubberised canvas as much as possible. This is done because initial distortion in the tube tends to further distort unevenly as the pressure is varied. The other end of the flexible coupling was fitted loosely (0·01 in. on diameter oversize) to the earthed supply ducting. Then with the internal pressure set at about 5 p.s.i. a quarter of an inch

section near the end of the flexible coupling was wound as tightly as possible by hand with 30 gauge steel wire. This was done to reduce the air-bearing gap to about 0·001 in. and to reinforce the rubberised canvas so that the gap did not increase as the pressure increased. The axial load on the model-support ducting was taken out on four (20 gauge) steel wires attached to the earthed supply ducting. The air loss through the air-bearing being bled from the main supply after the orifice plate, was calibrated as a function of internal pressure.

The flexible coupling, air-bearing connector described here was developed from the straightforward flexible coupling system, and it is reasonable to make some comparison of the performance with that described in Ref. 1. This comparison of the balance-zero errors caused is given in Table 1 which also gives the air loss through the air-bearing and the accuracy of repeatability of the corrections. The drag corrections are very small, and this has been achieved by adjustment of the flexible coupling. The present system could be improved further if the balance and supports were more rigid.

The calibrations of the balance-zero errors as shown in Table 1 were carried out every time the connector was removed or altered in any way and the appropriate correction applied to the balance readings. The balance zero was read at each incidence to allow for slight displacement of the earthed supply ducting which was rotated by a leadscrew device to follow the incidence change. This is the same system as was used during the calibration of the balance-zero errors for a range of pressures inside the coupling, where at each incidence the balance zero was read at zero pressure. As there is no stop valve after the flexible connector a plate was fitted to seal the open jet for the calibrations.

3.5. *Wind-Tunnel Corrections.* The corrections for tunnel wall interference when connected with high-lift, jet-blowing models are at present unknown[1]. To avoid the blockage correction the wind-tunnel velocity is measured with a pitot-static tube, which has been placed level with the model leading edge, 10 in. down from the tunnel roof and 16 in. out from the false tunnel wall, in accordance with the working-section calibration (Fig. 11). The model size is quite small in comparison with the tunnel working-section size (5 ft × 4 ft) and because of this all corrections are kept small. Only the two elementary corrections to incidence and drag are made, with the largest correction to incidence being less than two degrees for lift coefficients of four and only a small drag correction.

4. *Comparison of the Calibration Half-Model, and Full-Model Tests.* The half-model rig was calibrated using a flat-plate delta (aspect ratio one, and sharp leading edge) and comparing the lift, drag and pitching moment with similar full-model tests. This comparison is shown in Fig. 13, against the results of Tosti[7]. The two tests were carried out at the same tunnel speed but as the centre-line chord of the half model is 30 in. and the full model 39 in., the Reynolds numbers were $5{\cdot}2 \times 10^5$ and $6{\cdot}8 \times 10^5$ respectively. The full model was nominally a flat plate but the leading edge had a $\frac{3}{8}$ in. radius which accounts for the slightly lower non-linear lift contribution at higher incidences, as the development of the leading-edge vortex lags behind that from the strictly sharp leading edge. The empirical lift/incidence curve of Peckham[8] has been compiled from wind-tunnel data of several establishments for various aspect-ratio slender delta wings with sharp leading edges.

The comparison between half- and full-model tests is better than those illustrated by Van der Bliek[9], and this is undoubtedly due to the use of boundary-layer control on the false tunnel wall over the full length of the model. The effect of the boundary-layer control is shown clearly in Fig. 12 which illustrates two china-clay flow patterns on the flat-plate wing at incidence, one with the boundary-layer suction perforations sealed and the other with the boundary-layer suction in operation.

The overall comparison of the half- and full-model tests proved satisfactorily that the half-model rig would produce results directly comparable with full-model tests.

5. *Jets Arranged in a Spanwise Line.* The wind-tunnel testing started with an investigation into the effects of blowing from narrow spanwise slots at various chordal positions ($x_J = 0{\cdot}7$, $0{\cdot}8$ and $0{\cdot}9$). The general arrangement of these jets is given in the sketch of Fig. 14. It was hoped that some increased circulation effects could be gained in addition to the jet reaction, as is obtained with a jet flap or a split flap. It was realised that blowing forward of the trailing edge would produce an adverse low-pressure region behind the jet; but it is desirable for the jets to be located forward of the trailing edge to avoid large nose-down pitching moments. However, it was quickly established that blowing from any spanwise slot forward of the trailing edge does not give an increased circulation but rather a loss of wing lift. Fig. 15 shows the pressure distributions obtained for this configuration.

5.1. *Jet and Wing Interaction.* Before discussing the experimental results it is of interest to form an idea of what type of interaction will be caused by placing a slender wing at the source of a jet blown normally to a uniform stream.

Consider the source of the jet alone to be at some point in the uniform stream. The jet is emitted normally to the uniform stream and bends around until it is eventually flowing in the free-stream direction. There is a low-pressure region behind the jet, and it is the pressure difference across the jet stream which causes the bending into the free-stream direction where the pressures on either side become equal. It is this low-pressure region which also causes the cross-section of the jet to take on the 'horse-shoe' shape described by Jordinson[10]. The horse-shoe vortex is equivalent to the jet-edge vortex which (as will be shown later) forms at the edge of a flat jet sheet.

If a slender wing is now placed at the source of the jet, the free-stream air, which was previously flowing from above the jet into the low-pressure region now has to flow around the edge of the wing to reach this region. Considering the wing, this means that there is a lower pressure on the side of the wing behind the jet, and air tends to flow round the wing into this region.

5.2. *The Effect of Various Jet Parameters on the Lift, Drag and Pitching Moment.* Fig. 16 shows a comparison of the overall lift and drag coefficients for the spanwise jet slots at $x_J = 0{\cdot}7$, $0{\cdot}8$ and $0{\cdot}9$; for $C_\mu = 0$, 1 and 3. Before discussing these results it is important to refer to the pitching-moment coefficients for the same configurations, shown in Fig. 17. From these it is seen that the pitching moment with the jet slot at $x_J = 0{\cdot}9$ is $C_M = -0{\cdot}3$ for $C_\mu = 1{\cdot}0$. This is much too large to balance with a trailing-edge control surface, and for this reason only the results for the slots at $x_J = 0{\cdot}7$ and $0{\cdot}8$ will be considered in detail.

It can be seen from Fig. 16 that there is little difference between the performance of jet slots at $x_J = 0{\cdot}7$ and at $0{\cdot}8$, although the pitching moment for the jet slot at $x_J = 0{\cdot}8$ is higher and becomes large at about $C_\mu = 2$, whilst the pitching moment with jet slot at $x_J = 0{\cdot}7$ is satisfactory up to $C_\mu = 3$. Now the performance of these two configurations can be summed up by considering the case at zero wing incidence. At $C_\mu = 1$ the overall $C_L = 0{\cdot}17$, whereas if there were no adverse induced effects on the wing, a $C_L = 0{\cdot}866$ should be available as the vertical component of the jet reaction. This type of comparison can also be made with respect to the total thrust, with a similar large loss, in this case of the horizontal component of the jet reaction. It can be concluded that a spanwise jet slot is a very inefficient way of using jet engines to obtain increased lift; this is mainly due to the adverse interference effects of the jet on the latter part of the wing. The magnitude of this

interference is shown in the pressure distributions of Fig. 15, from which, for example, at $C_\mu = 1$ the drop in pressure on the lower surface behind the jet is of the order of four times the free-stream dynamic pressure. At $C_\mu = 3$ there is a complete reversal of pressure over the latter half of the wing with the pressure on the lower surface being lower than on the upper surface, which gives rise to flow from the upper surface to the lower surface discussed in the next section.

A comparison of the various jet exit area ratios is made in Fig. 18 for the spanwise jet slot at $x_J = 0{\cdot}7$. At $C_\mu = 1$ the variation of performance between $S_J/S = 0{\cdot}178$ per cent and $0{\cdot}711$ per cent is small, the order of 5 per cent in favour of the large area ratio, *i.e.*, the lower jet velocity. The better performance of the lower-velocity jet is clearly established at $C_\mu = 3{\cdot}0$ at which for $S_J/S = 0{\cdot}356$ per cent the jet velocity is about 1000 ft/sec and for $S_J/S = 0{\cdot}178$ per cent it is supersonic. Without going deeply into the effect of jet exit area on the results it may be stated that, as the jet speeds go above about half the speed of sound, then this becomes significant. The reason why the spanwise jet at various low velocities does not show much difference in lift and drag for a given value of C_μ is because a small amount of jet blowing induces large interference losses of wing pressure lift at low values of C_μ. This can be seen in Fig. 18 where a $C_\mu = 0{\cdot}5$ has produced no overall increase of lift, due to the loss of wing pressure lift cancelling out the vertical component of the jet reaction.

A spanwise row of six holes was tried as a jet exit at $x_J = 0{\cdot}7$ to compare with the rectangular slot. The overall lift and thrust was still low but slightly higher than for the continuous slot. This is probably due to free-stream air passing between the holes and slightly decreasing the suction induced on the wing behind the jet. When rows of 10 and 18 holes (*i.e.*, closer together) were tried the results were almost identical with those from the continuous slot.

Over the small range of Reynolds number tested ($5{\cdot}2 \times 10^5$ and $8{\cdot}35 \times 10^5$) there was little variation in the measured values of lift and drag.

With the spanwise jet slot at $x_J = 0{\cdot}9$ a comparison was made between a slot of length $l_J = 0{\cdot}183$ and one half this length ($l_J = 0{\cdot}0917$) of the same area ratio $S_J/S = 0{\cdot}178$ per cent and $\alpha_J = 60$ deg. An overall increase of lift of the order of 30 per cent was obtained with the shorter slot, with little change in thrust. By this time the cause of the low pressures behind the jet had been traced to the behaviour of the jet sheet vortex. The strength of the jet sheet vortex can be reduced by concentrating the jets into a group (*see* Section 6), which then interferes directly with a smaller area of the wing The shortening of the slot at $x_J = 0{\cdot}9$ was really a step in this direction.

5.3. *Flow Visualization, and Physical Behaviour of the Flow.* The behaviour of the flow over a slender delta wing with a spanwise jet, although steady, is of a fairly complex nature and five techniques have been used to explore it.

As soon as experiments began, using the spanwise jet slots, the resulting large loss of lift was measured. The model was fitted with 36 static-pressure holes (on both surfaces) and from these it was seen that the reason for the loss of lift was the low pressures induced behind the jet, as shown in Fig. 15. However, it was difficult initially to account for the extremely low pressure measured, and to complicate matters a vortex rotating in the opposite direction to the normal leading-edge vortex was picked up in a grid of wool tufts behind the wing. This is shown in Fig. 19 where a mirror is mounted behind the wool tufts and the photographs taken looking sideways at the tufts and straight down the core of the vortex through the mirror. In the top photograph the normal leading-edge vortex is shown, which is caused by the separation of the flow around the leading edge from the

lower to the upper surface. The lower picture shows the reverse vortex which is set up when the jet is blowing and which eventually completely swallows the normal leading-edge vortex as C_μ increases. The reverse vortex is caused by separation at the leading edge of the flow from the upper surface to the lower surface behind the jet.

The reverse vortex is perhaps best shown with some very slow-speed titanic chloride flow-visualization tests. A drop of titanic chloride on the wing emits a dense white vapour which will follow the streamline of a steady flow. The two top pictures of Fig. 20 illustrate the rolling up of the normal leading-edge vortex over the upper surface with no jet blowing. The two lower pictures with the jet blowing show the normal leading-edge vortex from the front travelling down over the upper surface of the wing and finally being drawn into the much stronger reverse vortex, separating from the latter section of the leading edge. A drop of titanic chloride was also put on the upper surface which illustrated a complete cross-flow across the wing, round the leading edge (not separating yet) and then being drawn into the jet. If the leading edges had been sharp there is no doubt that the separation of the reverse vortex would have been much earlier. The photographs were taken from outside the wind tunnel with complete darkness except for one beam (or slit) of light directed straight through the model from behind with no direct light falling on the blackened false tunnel wall behind.

The behaviour of the flow as so far described is further substantiated in Figs. 21 and 22, which are a series of china-clay flow patterns. These patterns are obtained by spraying on to the wing a thin mixture of paraffin (kerosene) and china clay (french chalk), and when the tunnel and jet are run at the required conditions the paraffin is swept away leaving a pattern in the deposited china clay which is further dried and photographed. The wing was painted red and photographed on ortho-chromatic film under ultra violet illumination; in this way it was possible to obtain a contrast between the white china clay and the wing which photographs black, there being little red light emitted from the ultra-violet source and the film not being sensitive to red light. The paraffin tends to get swept into low tangential-velocity areas such as the separation line of a vortex, and at the same time washing away a pattern in the china clay. It was difficult to obtain flow patterns on the underside of the wing (underside as it was suspended, *i.e.*, the upper surface of the wing).

Fig. 21 shows several china-clay patterns taken at 6 deg incidence for $C_\mu = 1$, 2 and 4. The patterns on the upper surface mainly illustrate the risk of misinterpretation of the photographs, as what looks to be a separation line is here mainly caused by the gravity effects. A lot of the paraffin has run round the leading edge and collected at the nearest low section of the wing, and as soon as the tunnel or boundary-layer bleed is switched on a large sheet of paraffin is swept off, carrying with it most of the china clay. However, the patterns on the lower surface are reliable and for example show that at $C_\mu = 2$ air is swept in a vortex motion behind the jet. There is a very low-pressure region behind the jet into which air flows round the leading edge from the upper surface, and at $C_\mu = 2$ flow separation has commenced, forming the reverse vortex. This is detected by the separation line of the reverse vortex forming near the leading edge at the back of the wing. At $C_\mu = 4$ this separation has become a complete washaway of the china clay near the leading edge. The whole strip is now a region of small shear stress, and it took about 10 minutes of tunnel running to remove the paraffin. Even after running some time a small pool of paraffin remains and spreads out forming the faint white strip which can be seen along the last few inches near the wing tip.

The experimental technique had been improved considerably when the patterns at 12 deg incidence (Fig. 22) were made. The upper surface does exhibit a definite attachment and washed

away separation line over the latter half of the wing caused by the normal leading-edge vortex. At 12 deg incidence this vortex is quite strong but even so at $C_\mu = 4$ it is seen to be distorted inwards and the establishment of the reverse vortex beginning.

The knowledge of the behaviour of the leading-edge vortices does not really explain the very low pressures behind the jet, they are in fact only the induced result of the low-pressure region. The explanation lay eventually in the behaviour of the jet sheet; the edge of which was found to roll up into an incredibly strong vortex. It was thought initially that most of the vortex on the edge of the jet (shown in Figs. 21 and 22 lower surface) was formed by the free-stream air, effectively separating around the edge of an obstruction. This however is incorrect as was shown immediately by a technique of water flow visualization, Fig. 23. Four $\frac{1}{8}$ in. (inside diameter) tubes were used to carry water into the lip of the jet exit where it was picked up and atomised by the jet. Following through the sequence of Fig. 23, it can be seen that at $C_\mu = 1$ the outer jet of water (representing 25 per cent of the jet) has curled round under the jet sheet and swept across the wing in a vortex-type path. This is shown in increasing intensity at $C_\mu = 3$ and 5. The two pictures taken parallel to the jet sheet show how the edge vortex completely breaks away from the jet sheet and follows its own path over the wing. This explains the very low negative pressures on the wing of the order of seven times the free-stream dynamic pressure at $C_\mu = 4$ (Fig. 15); because these pressures are pressures induced by jet velocities and as such should more fairly be related to the jet dynamic pressure ($\frac{1}{2}\rho v_J^2$). However, the result is that the jet sheet vortex has the velocities of the jet and not the free stream and is strong enough to influence greatly the flow over the entire wing. The jet sheet vortex does not seem to exist for long, because after barely one revolution it appears to become turbulent and is not picked up as a vortex on the tuft grid behind the wing. It is the reverse vortex which eventually comes out the steadiest and best established, to be detected quite clearly on the tuft grid.

It is interesting to note in Figs. 21 and 22 that after the first half turn, the jet sheet vortex lifts clear of the wing and free-stream flow (and its associated pressures (Fig. 15)) are re-established again near the trailing edge, and it is only at the highest C_μ values tested that the jet sheet-vortex interference reaches the trailing edge. This will later prove to be very important when trying to use trailing-edge controls.

To conclude this description of the physical nature of the flow, it could be said that any jet blown from the lower surface of a forward moving wing will try to behave in much the same manner as the flat jet sheet. However, if the jet is more concentrated in a solid block, the edges of the jet sheet roll up in a vortex more slowly, and the induced pressures behind the jet are reduced in magnitude.

6. *Jets Grouped Near the Centre-line of the Wing.* Following the investigation of the effect of spanwise jet sheets it was decided to find out if any improvement in performance could be gained by grouping the jets in a block near the centre-line. Two reasons prompted this grouping of the jets: (*a*) less of the wing area came directly under the adverse effects of the jet-edge vortex, (*b*) reduction of the jet width and hence area, reduced the normal force on the jet and the consequent strength of the jet-edge vortex.

At this stage of the overall investigation of blowing from a slender delta wing it was realised that no increased circulation could be induced by a jet blown well forward of the trailing edge, in fact it was now rather the case of trying to reduce the adverse interference of the jet to maintain stability and to obtain as much of the component of the jet reaction as possible.

The configuration of the jets grouped near the centre-line is shown in Fig. 14. The jets were tested at $x_J = 0{\cdot}7$ and $0{\cdot}8$ for $\alpha_J = 30$ deg and 60 deg. Tests were also carried out with a trailing-edge elevator control and for ground interference.

6.1. *Effect of Various Parameters on the Lift and Drag.* Fig. 24 shows the overall lift and drag coefficients of the wing for the jets grouped near the centre-line at $x_J = 0{\cdot}7$ with $S_J/S = 0{\cdot}356$ per cent and for $\alpha_J = 30$ deg and 60 deg. The lift and drag coefficients for the jets at $x_J = 0{\cdot}8$ were very similar but slightly less as can be seen in Fig. 25, which shows the overall lift and drag coefficients for the jets at $x_J = 0{\cdot}7$ and $0{\cdot}8$ as a function of the jet momentum coefficient, C_μ. It is seen that the overall lift and drag coefficients vary linearly with C_μ for values of $C_\mu > 1$. Below $C_\mu = 1$ the drag, or rather thrust, approaches a 100 per cent thrust recovery of the horizontal component of the jet reaction, whilst the lift recovery falls a little. To put these results into a usable form and to see the effect of various parameters a set of empirical equations have been derived.

The equations are derived for the overall lift and drag coefficient of a wing with assisting jets grouped near the centre-line at $x_J = 0{\cdot}7$, blowing with values of between $C_\mu = 0{\cdot}25$ and $3{\cdot}0$. In practice, take-off values of C_μ are not likely to be greater than unity.

Firstly the equation for the overall lift coefficient, which is basically an expression derived from the two sources of lift, *i.e.*, the pressure lift and the jet reaction component. We have $C_L = C_{L(\text{wing alone})} + C_{L(\text{due to jet})}$. The lift for the wing alone was found to be:

$$C_{L(\text{wing alone})} = \{2\sqrt{2}\alpha + 3\alpha^2\}\sqrt{\left(\frac{s}{c_0}\right)} \tag{1}$$

where

s Wing semi-span

c_0 Wing root chord

α Wing incidence to the free-stream direction.

This equation shows that the separation from the round leading edge of the model tested, produced a non-linear increment of $3\alpha^2$ in comparison with the $4\alpha^2$ produced by a strictly sharp leading edge[8].

Now to the first order, neglecting all interference effects, the contribution of the jet reaction to the lift would be

$$C_{L(\text{jet react.})} = C_\mu \sin(\alpha_J + \alpha) \tag{2}$$

However, the total component of the jet reaction is not achieved due to interference effects. We begin by considering this interference at zero wing incidence. For $C_\mu > 1$ the overall C_L at zero incidence is a linear function of C_μ (Fig. 26). The interference corrections to overall C_L for change of jet angle α_J are also assumed to be linear, although measurements were only made for $\alpha_J = 30$ deg and 60 deg. At zero incidence the fraction of C_μ which is realised as lift can be expressed as:

$$C_{L(\text{jet react.})\,(\alpha=0)} = C_\mu \left\{0{\cdot}9 - 0{\cdot}286\left(\frac{\pi}{2} - \alpha_J\right)\right\} \sin\alpha_J . \tag{3}$$

If this linear approximation for the effect of α_J can be extended above $\alpha_J = 60$ deg, then the indication is that the maximum amount of jet reaction obtainable as lift at zero incidence at $\alpha_J = 90$ deg, for the jet area ratio used is, lift $= 0{\cdot}9 \times$ jet reaction.

Combining equations (1), (2) and (3), the overall C_L for $1{\cdot}0 \leqslant C_\mu \leqslant 3{\cdot}0$ can be expressed as

$$C_L = \{2\sqrt{2}\alpha + 3\alpha^2\}\sqrt{\left(\frac{s}{c_0}\right)} + C_\mu \sin(\alpha_J + \alpha)\left\{0{\cdot}9 - 0{\cdot}286\left(\frac{\pi}{2} - \alpha_J\right)\right\}. \tag{4}$$

Now for the range $0{\cdot}25 < C_\mu < 1{\cdot}0$ there are several non-linear effects which have to be added, because at low values of C_μ the forces induced by interference effects are of the same order as the jet reaction. No attempt will be made to apply the resulting equation for values below $C_\mu = 0{\cdot}25$, as few measurements of lift in this non-linear range were made.

Below $C_\mu = 1$ the slope of the overall lift curve (C_L/α) rapidly approaches that of the wing alone, C_L does not increase linearly with α, and equation (2) is replaced by

$$C_{L(\text{jet react.})} = C_\mu \sin(\alpha_J + C_\mu{}^2\alpha). \tag{5}$$

Also the value of C_L at zero incidence is affected, and equation (3) for C_L at zero incidence is modified to

$$C_{L(\text{jet react.})\,(\alpha=0)} = \frac{(C_\mu - 0{\cdot}1)}{0{\cdot}9}\left\{0{\cdot}9 - 0{\cdot}286\left(\frac{\pi}{2} - \alpha_J\right)\right\}\sin\alpha_J. \tag{6}$$

Combining equations (1), (5) and (6) the overall C_L for $0{\cdot}25 < C_\mu < 1{\cdot}0$ can be expressed as

$$C_L = \{2\sqrt{2}\alpha + 3\alpha^2\}\sqrt{\left(\frac{s}{c_0}\right)} + \frac{(C_\mu - 0{\cdot}1)}{0{\cdot}9}\sin(\alpha_J + C_\mu{}^2)\left\{0{\cdot}9 - 0{\cdot}286\left(\frac{\pi}{2} - \alpha_J\right)\right\}. \tag{7}$$

A similar approach has been used to obtain an expression for the overall drag. If there were no interference effects the drag could be expressed as the sum of the two sources

drag = drag of the wing alone − component of jet reaction.*

For the wing alone, the graph of C_D against $C_L{}^2$ is linear hence giving a convenient expression for C_D of the wing alone.

$$C_{D(\text{wing alone})} = 0{\cdot}017 + 0{\cdot}446C_L{}^2{}_{(\text{wing alone})} = 0{\cdot}017 + 0{\cdot}446\frac{s}{c_0}\{2\sqrt{2}\alpha + 3\alpha^2\}^2. \tag{8}$$

At zero incidence up to $C_\mu = 1$ the thrust component of the jet reaction is completely realised, giving

$$C_{T(\alpha=0)} = C_\mu \cos\alpha_J \tag{9}$$

where C_T is the thrust coefficient of assisting jet. However, with incidence the thrust recovery is less than a linear increase with added incidence, α and is given by

$$C_T = C_\mu \cos(\alpha_J + 0{\cdot}8C_\mu\alpha) \tag{10}$$

Combining equations (8) and (10), the overall C_D for $0{\cdot}25 < C_\mu \leqslant 1{\cdot}0$ can be expressed as

$$C_D = 0{\cdot}017 + 0{\cdot}446\frac{s}{c_0}\{2\sqrt{2}\alpha + 3\alpha^2\}^2 - C_\mu \cos(\alpha_J + 0{\cdot}8C_\mu\alpha) \tag{11}$$

For $C_\mu > 1$ the thrust recovery is less than 100 per cent of the component of the jet reaction and a correction proportional to $(C_\mu - 1)$ arises. Also the effect of incidence is now dependent on $0{\cdot}8\alpha$ (not $0{\cdot}8\ C_\mu\alpha$ as for $C_\mu < 1$). The thrust minus the correction is now given by

$$C_T = C_\mu\cos(\alpha_J + 0{\cdot}8\alpha) - 0{\cdot}15(C_\mu - 1)\cos(\alpha_J + 0{\cdot}8\alpha) = \{0{\cdot}85C_\mu + 0{\cdot}15\}\cos(\alpha_J + 0{\cdot}8\alpha). \tag{12}$$

* N.B. The jet reaction is considered positive when the jet is directed rearwards.

Combining equations (8) and (12), the overall C_D for $1{\cdot}0 < C_\mu < 3{\cdot}0$ can be expressed as

$$C_D = 0{\cdot}017 + 0{\cdot}446\frac{s}{c_0}\{2\sqrt{2}\alpha + 3\alpha^2\}^2 - \{0{\cdot}85C_\mu + 0{\cdot}15\}\cos(\alpha_J + 0{\cdot}8\alpha). \tag{13}$$

A comparison of the empirical equations for overall lift and drag coefficients with the experimental results is given in Figs. 26 and 27.

These empirical equations for overall lift and drag of a wing with assisting jets grouped near the wing centre-line are summarised, with limitations of their use, below:

For $0{\cdot}25 < C_\mu \leqslant 1{\cdot}00$

$$C_L = C_{L(\text{wing alone})} + \frac{(C_\mu - 0{\cdot}1)}{0{\cdot}9}\sin(\alpha_J + C_\mu{}^2\alpha)\left\{0{\cdot}9 - 0{\cdot}286\left(\frac{\pi}{2} - \alpha_J\right)\right\} \tag{14}$$

$$C_D = C_{D(\text{wing alone})} - C_\mu\cos(\alpha_J + 0{\cdot}8C_\mu\alpha). \tag{15}$$

For $1{\cdot}00 \leqslant C_\mu < 3{\cdot}00$

$$C_L = C_{L(\text{wing alone})} + C_\mu\sin(\alpha_J + \alpha)\left\{0{\cdot}9 - 0{\cdot}286\left(\frac{\pi}{2} - \alpha_J\right)\right\} \tag{16}$$

$$C_D = C_{D(\text{wing alone})} - \{0{\cdot}85C_\mu + 0{\cdot}15\}\cos(\alpha_J + 0{\cdot}8\alpha). \tag{17}$$

Strictly these equations should only be applied over the range of variables covered by the experiments. However, the ranges of applicability may be extended a little (where the effects are known to be either small or orderly) in the following respects:

(1) The wing could be replaced by a gothic shape or cropped delta as long as the semi-span to centre-line chord ratio was within the limits $\frac{3}{16} < s/c_0 < \frac{5}{16}$.

(2) The equations are not valid for values of C_μ less than $C_\mu = 0{\cdot}25$, but an extension to $C_\mu = 5{\cdot}0$ is satisfactory if it should ever be needed.

(3) The range of α_J can be taken safely to 75 deg but not below 25 deg, as the interference effects of the jet nearer the wing are quite unknown (angles of α_J about 30 deg are very inefficient and would not be used anyway).

(4) There was no Reynolds number effect detected over the small range tested ($5{\cdot}20 \times 10^5$ and $8{\cdot}35 \times 10^5$). At low subsonic speeds Reynolds number is only critical if the boundary-layer transition varies greatly or if there is a different position of a boundary-layer separation. If these do not occur then the equations are quite applicable to full scale, and it is not expected that either of them would occur on a slender wing which has flow separation from the leading edge at all relevant Reynolds numbers.

(5) The majority of the experiments were carried out using a jet area ratio of $S_J/S = 0{\cdot}356$ per cent, and although other area ratios were used no conclusion could be drawn as to the exact effect of varying the jet area ratio. This was due to the spacing of the centre of the four jet exit holes on the model being the same for different jet area ratios. Hence being on the same spacing they interfered directly with nearly the same area of wing behind the jet. However, the empirical equations could be used safely up to an area ratio of $S_J/S = 1{\cdot}0$ per cent without incurring any large error, as long as they were applied to conventional jet engines.

The one particular point of interest which arises from the limitations of the empirical equations is the fall-off in efficiency of the lift obtained as the jet angle α_J is reduced {equation (3)}. This is

almost certainly due to the increase of suction on the wing behind the jet, as the jet efflux approaches the surface. This characteristic is most unfortunate as it means that it is very inefficient to try and assist the lift and thrust at the same time, and it has been shown in performance estimates that blowing a jet at an angle of $\alpha_J = 30$ deg produces virtually no decrease in take-off speed, as the increased lift is cancelled by the extra weight of the engines and the fuel etc. required to carry them over a long range.

6.2. *Effect of Various Parameters on the Pitching Moment.* Figs. 28a and 28b show the overall pitching-moment coefficients as a function of lift coefficient for the jets grouped near the centre-line. The pitching-moment coefficients are based on the aerodynamic mean chord ($\frac{2}{3}c_0$) and are taken about the quarter-chord point of the aerodynamic mean chord ($x = 0{\cdot}5$). Fig. 29 shows the pitching-moment coefficient as a function of the jet momentum coefficient (C_μ) when the wing incidence is zero.

The effect of a trailing-edge control surface is discussed more fully in Section 6.4, but it has been shown in Ref. 14 that a trailing-edge control surface can adequately cope with changes of C_μ between zero and unity with the grouped jets at $x_J = 0{\cdot}7$. The same is true to a slightly lesser extent for the jet at $x_J = 0{\cdot}8$, where when the jet is at $\alpha_J = 60$ deg and approaching $C_\mu = 1$ then the use of a trailing-edge control surface is probably at the limit.

The most interesting effect that the jet has on the pitching moment is not so much the magnitude produced, but the adverse effect that the jet has on the static margin. The magnitude of the pitching moment can be controlled by correct positioning of the jet, but the effect on dC_M/dC_L appears to be relatively independent of the two jet positions and jet angles tested (*i.e.*, $x_J = 0{\cdot}7$ and $0{\cdot}8$, and $\alpha_J = 30$ deg and 60 deg). This effect can be stated generally as follows: the value dC_M/dC_L is greater when the jet is blowing than for a wing alone (*i.e.*, the value dC_M/dC_L becomes less negative), which means that the static margin is reduced when the jet is blowing.

Instead of showing dC_M/dC_L as a function of C_μ, a set of figures (Fig. 30) have been drawn to show the static margin as a function of C_μ. The static margin used is based on the centre-line chord (c_0) and the centre of gravity is taken to be at $x = 0{\cdot}6$. By showing the static margin based on c_0 it is possible to quickly see what the static margin is for other centre of gravity positions.

The static margin is constant for various wing incidences up to $\alpha = 12$ deg; as the incidence increases then without exception the static margin increases. Hence in Fig. 30 two lines are drawn, one for -4 deg $< \alpha < 12$ deg and the other for $\alpha = 16$ deg. This effect can be observed in Figs. 28a and 28b. The magnitude of the loss of static margin for incidences up to $\alpha = 12$ deg could be stated generally as going from + 3 per cent for no jet (*i.e.*, $C_\mu = 0$) to zero for $C_\mu = 0{\cdot}5$.

There is no regular relation which controls the adverse effect of the jet on the static margin although the cause would seem to be the jet interaction on the wing. That is to say that the low pressures induced on the lower surface of the wing behind the jet produce a pitching moment which opposes that produced by the direct reaction of the jet on the wing. Hence the nose down pitching moment does not increase with incidence, for pressure plus jet lift, at the same rate as does a wing which has no jet lift.

6.3. *Ground Interference.* A short investigation into the ground interference effects was made with the grouped jets blowing from $x_J = 0{\cdot}7$ at $\alpha_J = 60$ deg and 30 deg and the results shown in Fig. 31. Unfortunately, testing ground interference with a half model is not very satisfactory due to the build up of the boundary layer in the corner between the false wall and the ground board,

discussed by Gersten[11]. Because of this interference the comparison between half-model and the full-model results of Kirby and Peckham[12] is not very good. For the wing alone at 15 deg incidence the increase of lift due to moving the wing from $d/\bar{\bar{c}} = 0{\cdot}75$ to $0{\cdot}25$ for the half model is 17 per cent, whereas that from the full model is of the order of 26 per cent, where d is the distance of the centre of the model at $x = 0{\cdot}5$ from the ground and $\bar{\bar{c}}$ is the aerodynamic mean chord ($\bar{\bar{c}} = \frac{2}{3} c_0$). One other factor which does influence this comparison is that the half model has a rounded leading edge and the full model has a sharp leading edge, and so the latter has a stronger leading-edge vortex, which produces a greater increase of lift due to ground interference, but not of the order of the difference in the comparison.

However, the result from the half model can be used to compare the effects of ground interference with the jet blowing, although it would be inaccurate to use the results quantitatively.

The main reason for the investigation was to find out if any of the adverse recirculation (or vortex) effects existed in front of the jet as described by Huggett[13] in his two-dimensional work on jet flaps. Using the china-clay flow-visualization method no indication of any recirculation in front of the jet was detected with the slender delta using the grouped jets, and in fact it would seem that this recirculation is basically a two-dimensional effect.

More important though is the overall effect of the ground interference (Fig. 31 and the following Table).

Approximate percentage increase or decrease of lift due to ground effect between $d/\bar{\bar{c}} = 0{\cdot}75$ and $0{\cdot}25$

α_J \ C_μ	0·5	1·0	3·0
30°	0% at $\alpha = 0$ 10% dec. at $\alpha = 15°$	0%	5% inc.
60°	17% inc. (Same as for the wing alone)	10% inc. at $\alpha = 15°$ 8% dec. at $\alpha = 0°$	15% dec.

With a jet angle of 60 deg and up to $C_\mu = 0{\cdot}5$ the jet produces the same percentage increase of lift as the wing alone. At $C_\mu = 1{\cdot}0$ the percentage increase is less and at low incidences the effect of the ground was to reduce the lift slightly. At $C_\mu = 3{\cdot}0$ the adverse effect of the ground is quite large, there now being a 13 per cent loss of lift between $d/\bar{\bar{c}} = 0{\cdot}75$ to $0{\cdot}25$ at 15 deg incidence. However, as take-off values of C_μ are likely to be about $0{\cdot}5$, for $\alpha_J = 60$ deg, it could be concluded for all practical purposes that the ground interference on the lift with the jet blowing is the same as for the wing alone. The drag (or thrust) is very little affected up to $C_\mu = 1{\cdot}0$ and hence there is a significant increase in lift/drag ratio.

For the jet angle $\alpha_J = 30$ deg a very different picture exists. Up to $C_\mu = 1{\cdot}0$ the effect of ground interference on the wing at 15 deg incidence is to reduce the lift, whilst at $C_\mu = 3{\cdot}0$ there is a slight increase of lift. This is yet another of the adverse characteristics which arise when the jet is blown at angles approaching 30 deg to the wing plane.

The effect of the ground interference on pitching moment is very favourable, particularly at high incidence. The pitching-moment coefficients about the quarter-chord point of the aerodynamic

mean chord ($x = 0{\cdot}5$) are shown in Fig. 31. The slope dC_M/dC_L is decreased under all blowing conditions up to $C_\mu = 1{\cdot}0$ in much the same manner as for the wing alone. This decrease of dC_M/dC_L and hence increase of the static margin is very useful for the jet-on case, as the tendency in free flight is for the jet to decrease the static margin.

6.4. *Effect of a Trailing-Edge Control Surface.* An investigation of the flow in the region of the trailing edge with the jet blowing was made using the china-clay flow-pattern technique. This was to determine if it would be possible to use a trailing-edge control, and as can be seen in the patterns (Fig. 33) the flow near the entire trailing edge is steady and mostly parallel to the free-stream direction. Following the flow investigation a short series of tests were made with a trailing-edge control surface, or elevator. The elevator was hinged at $x = 0{\cdot}95$, extended to the wing trailing edge, and extended spanwise from $y = 0{\cdot}05$ to $y = 0{\cdot}20$. The jet was blown at an angle $\alpha_J = 30$ deg as this case would cause more interference with the wing than for $\alpha_J = 60$ deg, and as such was a better test of the effectiveness of a trailing-edge control.

The pitching-moment coefficient, taken about the mean aerodynamic quarter-chord point, is plotted against lift coefficient in Fig. 32. Three characteristics are worth commenting upon, apart from the fact that the elevator works as well with jets on as with jets off.

(1) The slope dC_M/dC_L is increased as C_μ is increased, which effectively means a reduction in static margin.

(2) For incidences up to 10 degrees the effectiveness of the elevator is increased as C_μ increases, *i.e.*, at an elevator angle of $\eta = 20$ deg the pitching-moment difference from $\eta = 0$ for $C_\mu = 1$ is 25 per cent greater than for $C_\mu = 0$.

(3) For incidences above 10 degrees the elevator effectiveness is initially reduced by the jet, but it does not get worse as C_μ increases.

7. *Vertically Directed Jets in a Chordwise Line.* A series of tests were carried out with a jet blown from a chordwise slot near the centre-line. The jet was nominally directed vertically down to simulate the proposal of A. A. Griffith for a row of jets for a vertical take-off aircraft. The actual angle α_J was 87·5 degrees, this being the slope of the wing surface onto which the jet exit slot was fixed. The chordwise slot was located centrally about $x = 0{\cdot}61$ which is the centre of pressure and aerodynamic centre for the plain wing. This was not meant in any way to be a full investigation of the vertical take-off characteristics but just an investigation into the lift drag and pitching moment which would occur towards the end of the transitional flight from vertical to horizontal while the aircraft is still partially jet supported.

The results given in Fig. 34 are not very encouraging from an efficiency point of view. The lift coefficient obtained at zero incidence is between 65 per cent and 70 per cent of the jet momentum coefficient, which is only just better than the lift component of the reaction of the jets grouped near the centre-line blowing at an angle $\alpha_J = 60$ deg. Hence for lifting alone the chordwise slot is rather inefficient and considerable improvement could be made by grouping the jets together.

The pitching-moment coefficient (Fig. 34) is taken about $x = 0{\cdot}61$, the wing aerodynamic centre, to give some idea of the trim requirements. The pitching-moment difference between $\alpha = 0$ deg and 8 deg is such that the moments to trim are high but not excessive. The pitching moment about the aerodynamic centre is positive for nearly all cases and so with the centre of gravity forward of $x = 0{\cdot}61$ the static margin is positive, although very small at low values of lift coefficient.

8. *Jet Flap.* An investigation was made of the effects of blowing from the trailing edge of a flap hinged at $x_J = 0{\cdot}9$ with an angle $\alpha_J = 60$ deg. The flap was the same length as the spanwise jet slot at $x_J = 0{\cdot}9$, *i.e.*, extending from $y = 0{\cdot}0083$ to $0{\cdot}192$ (*i.e.*, 74 per cent of the trailing edge). The area ratio of the slot was $S_J/S = 0{\cdot}356$ per cent. The results are given in Fig. 35.

The flap alone was large, having a chord equal to $0{\cdot}1\,c_0$ and at zero incidence with flap down and jet off the wing had a lift coefficient of $C_L = 0{\cdot}31$. At zero incidence with the jet on at $C_\mu = 0{\cdot}5$ the lift coefficient was $C_L = 1{\cdot}44$, which indicates a large increase of pressure lift on the wing due to the supercirculation. This increase of lift is in contrast to the small increase of lift obtained when a jet of the same parameter was blown directly from $x_J = 0{\cdot}9$, under which conditions the lift coefficient was $C_L = 0{\cdot}32$.

Fig. 35 shows, as expected, that there is a large negative pitching moment with the jet flap in operation at $C_\mu = 1{\cdot}0$.

9. *Conclusions.* The conclusions drawn from the experiments on jet blowing from a delta wing are summarised in the following list.

1. A spanwise jet located far enough forward of the trailing edge to avoid large nose-down pitching moments gives rise to no supercirculation, but rather induces a large loss of lift due to the low-pressure region behind the jet.

2. The jets grouped near the centre-line are much more efficient, but it is unlikely that the lift realised from the jet will be over 90 per cent of the component of the jet reaction.

3. For a jet angle (α_J) about 60 deg the component of thrust realised is 100 per cent for values of $C_\mu < 1{\cdot}0$.

4. Using a jet angle (α_J) of 30 deg is very inefficient and only about 60 per cent of the component of the jet reaction is realised as lift.

5. The ground effect for the jet at $\alpha_J = 60$ deg and $C_\mu < 0{\cdot}5$ is the same as for the wing alone. (No quantitative figures are quoted on this, because using a ground board with a half-model technique is not at all satisfactory, although the general trend was observed.)

6. A trailing-edge control surface can provide adequate pitching moments to trim the aircraft with the jets blowing from $x_J = 0{\cdot}7$.

7. A spanwise row of jets proved to be very inefficient; the grouped jets being far superior.

Acknowledgements. The author would like to express his thanks to the late Prof. H. B. Squire for advice given during the experimental work and the preparation of the thesis.

NOTATION

x, y, z — Non-dimensional Cartesian co-ordinates based on c_0 with the origin at the apex of the wing, x lying along the wing centre-line and z normal to the chordal plane of the wing (Fig. 1)

A — Aspect ratio, $4s/c_0$

a — Speed of sound

C_D — Overall drag coefficient, $\dfrac{\text{Drag}}{\frac{1}{2}\rho_0 V_0^2 S}$

C_L — Overall lift coefficient, $\dfrac{\text{Lift}}{\frac{1}{2}\rho_0 V_0^2 S}$

C_M — Overall pitching-moment coefficient, referred to aerodynamic mean chord, taken about the mean quarter-chord, $\dfrac{\text{Pitching Moment}}{\frac{1}{2}\rho_0 V_0^2 S\bar{c}}$

C_P — Pressure coefficient, $\dfrac{p_0 - p_s}{\frac{1}{2}\rho_0 V_0^2}$

C_T — Thrust coefficient of the assisting jet

C_μ — Jet momentum coefficient, $\dfrac{(m_J/g)v_J}{\frac{1}{2}\rho_0 V_0^2 S}$

c — Wing chord

c_0 — Wing chord at the centre section (= unity)

$\bar{c}$ — Geometric mean chord, $c_0/2$

$\bar{\bar{c}}$ — Aerodynamic mean chord, $\displaystyle\int_{-s}^{s} c^2\,dy \Big/ \int_{-s}^{s} c\,dy$

d — Distance of the mid-centre-line chord point above the ground

g — Acceleration due to gravity

J — Subscript for jet conditions or parameters (Fig. 1)

m_J — Measured mass flow of the jet

o — Subscript for free-stream conditions

p_D — Stagnation pressure in the wing plenum chamber

p_0 — Free-stream static pressure

p_s — Static pressure

R — Reynolds number (based on $\bar{\bar{c}}$)

NOTATION—*continued*

R_{xw}	Reynolds number (based on x_w)
S	Wing area
S_J	Jet exit area
$S_{(x)}$	Cross-sectional area
s	Wing semi-span
V_0	Free-stream velocity
v_J	Theoretical jet velocity reached on isentropic expansion from the stagnation pressure p_D in the wing plenum chamber to free stream p_0
x_J	x co-ordinate of the centre of the jet on the wing chordal plane
y_J	y co-ordinate of the centre of the jet on the wing chordal plane
α	Wing incidence to the free-stream direction
α_J	Exit angle of the jet stream to the chordal plane of the wing
δ	Theoretical boundary-layer thickness
η	Angle between the elevator and the chordal plane of the wing
ν	Non-dimensional volume of the wing based on c_0^3
ρ	Density
ρ_0	Free-stream air density

REFERENCES

No.	*Author*	*Title, etc.*
1	A. Anscombe and J. Williams ..	Some comments on high-lift testing in wind tunnels with particular reference to jet blowing models. *J. R. Ae. Soc.*, No. 560. Vol. 61. August, 1957.
2	K. H. Doetsch	The time vector method for stability investigations. A.R.C. R. & M. 2945. August, 1953.
3	W. T. Lord and Miss B. Green ..	Some thickness distributions for narrow wings. A.R.C. 19,459. February, 1957.
4	J. Weber	Slender delta wings with sharp edges at zero lift. A.R.C. 19,549. May, 1957.
5	——	Flow measurement. British Standards Specification No. 1042. 1945.
6	R. C. Pankhurst and D. W. Holder	*Wind tunnel techniques.* Sir Isaac Pitman & Sons Ltd., London. 1952.
7	L. P. Tosti	Low-speed static stability and damping-in-roll characteristics of some swept and unswept low-aspect-ratio wings. N.A.C.A. Tech. Note 1468. October, 1947.
8	D. Peckham	Unpublished R.A.E. investigation.
9	J. A. van der Bliek	Notes on half-model testing in wind tunnels. N.A.E. Canada L.R.–235. A.G.A.R.D. Report 298. 1959.
10	R. Jordinson	Flow in jets normal to a stream. Unpublished thesis. Imperial College, London University, March, 1956.
11	K. Gersten	Corner interference effects. A.G.A.R.D. Report 299. March, 1959.
12	D. A. Kirby and D. H. Peckham	Unpublished work at the R.A.E. on ground interference.
13	D. J. Huggett	The ground effect on the jet flap in two dimensions. *Aero. Quart.* Vol. X. Part I. February, 1959.
14	W. H. Melbourne	Experiments on a delta wing with jet-assisted lift. Unpublished thesis. Imperial College, London University, February, 1960.

APPENDIX

Derivation of Constant Thickness/Chord Ratio Delta Wing with a Lord V Area Distribution

As described in Section 2.1 the half model used for the wind-tunnel test was a constant thickness/chord ratio delta wing, which had approximately an area distribution known as the Lord V, which is an area distribution based on drag calculations using the linearised slender-body theory[3,4]. The derivation of the exact profile co-ordinates is as follows:

From Ref. 3 the Lord V area distribution is given as the following polynomial:

$$S_{(x)} = 7\nu x^2(1-x)\{4 - 6x + 4x^2 - x^3\} \tag{1A}$$

where

$S_{(x)}$ Cross-sectional area

ν Non-dimensional volume of the wing based on c_0^3

x, y, z Non-dimensional Cartesian co-ordinates based on c_0 with the origin at the apex of the wing, x lying along the wing centre-line and z normal to the chordal plane of the wing

c_0 Wing centre-line chord.

Equation (1A) can be expanded to

$$S_{(x)} = 7\nu(\mu - \mu^2 - \mu^5 + \mu^6) \tag{2A}$$

where $\mu = (1-x)$. Now the cross-sectional area ($S_{(x)}$) at any distance x from the apex can be expressed as

$$S_{(x)} = 4\int_0^{sx} z(xy')dy' \tag{3A}$$

where

$z(xy')$ z co-ordinate at a point x, y'

s Semi-span.

Now for a delta wing

$$z(xy') = z(x')\left\{\frac{1-x}{1-x'}\right\}$$

and

$$\frac{y'}{s} = \frac{x-x'}{1-x'}$$

where $z(x')$ is the co-ordinate at $y = 0$ (*i.e.*, the centre section). Hence equation (3A) becomes

$$\begin{aligned} S_{(x)} &= -4s\int_0^x z(x')\frac{(1-x)^2}{(1-x')^3}dx' \\ &= 4s(1-x)^2\int_1^{\mu} z(x')\frac{1}{\mu'^3}d\mu' \end{aligned} \tag{4A}$$

with $\mu' = 1 - x'$. The solution for this equation with $S_{(x)}$ given by equation (2A) is

$$z_{(x')} = (\mu + 3\mu^5 - 4\mu^6)\frac{7\nu}{4s} \tag{5A}$$

This is the equation of the centre section of a constant thickness/chord ratio wing with a Lord V area distribution.

TABLE I

Comparison of typical zero distortion errors caused by the flexible coupling, air-bearing system and those of a straightforward flexible coupling as published in Ref. 1

Model incidence (degrees)	Pressure (inches of mercury)	Straightforward flexible coupling (Ref. 1)			Flexible coupling, air-bearing		
		Lift (lb)	Drag (lb)	Pitching moment (lb ft)	Lift (lb)	Drag (lb)	Pitching moment (lb ft)
0	30	1·7	3·39	1·9	0·19	0·109	0·09
	60	4·7	3·77	4·8	0·34	0·048	0·19
16	30	2·3	2·54	2·0	0·24	−0·004	0·08
	60	5·6	3·30	4·4	0·36	−0·055	0·24

Accuracy of repeatability for the flexible coupling, air-bearing

Lift ± 0·02 lb

Drag ± 0·03 lb

Pitching Moment ± 0·02 lb ft

Typical calibration for the loss of air through the air-bearing gap

Pressure (in. mercury)	20	40	60
Mass flow (lb/sec)	0·026	0·046	0·064

Accuracy of repeatability ± 0·002 lb/sec

Jet position is defined by x_J, y_J the centre of the jet.

The type and size of jet is defined by ω_J, l_J and if circular then also by the number of circular jets n_J and the radius r_J

The angle of the jet centre-line to the wing plane is a_J.

Wing area is S.

Jet area is S_J.

All lengths are non-dimensionalised, based on C_o.

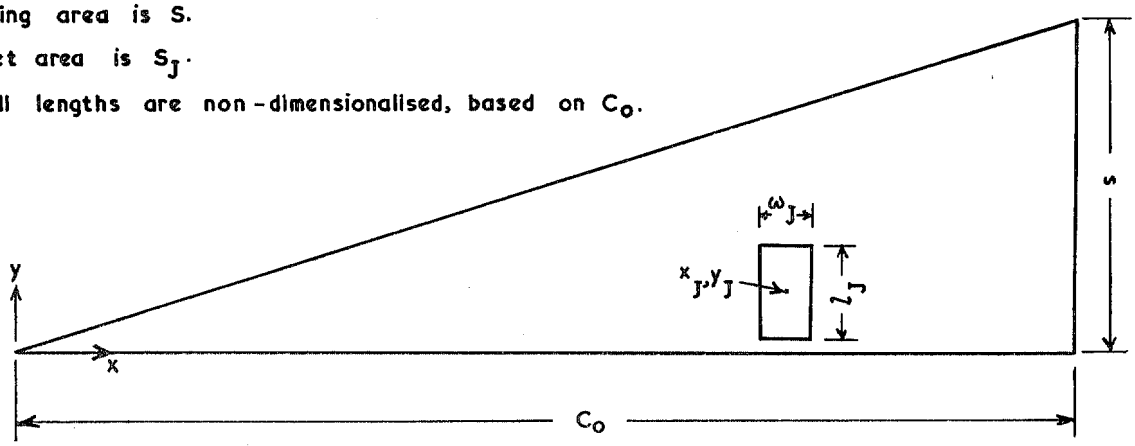

FIG. 1. The co-ordinate system, and nomenclature to define the jet position and size.

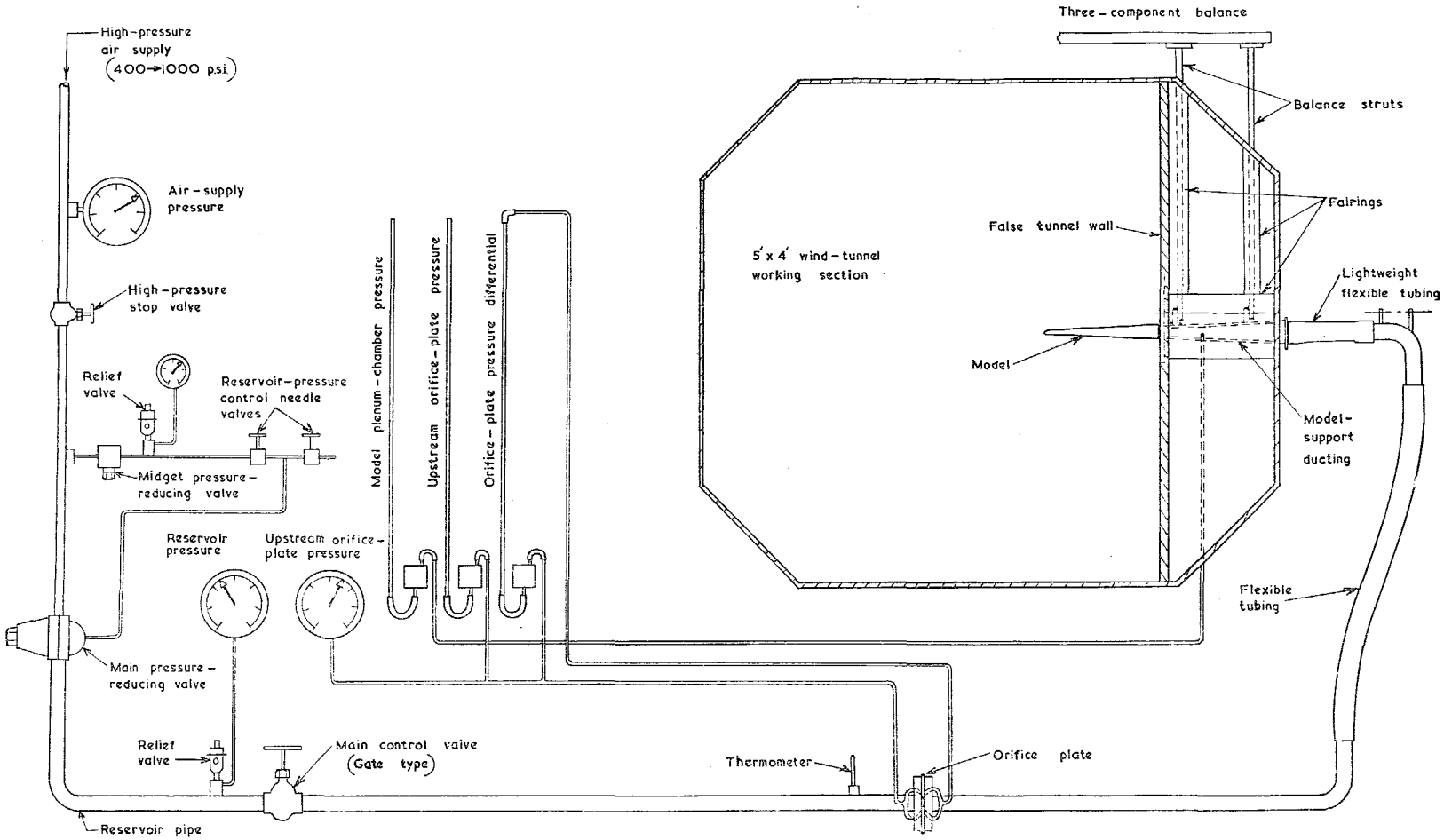

FIG. 2. General arrangement of the model-support system and the air supply.

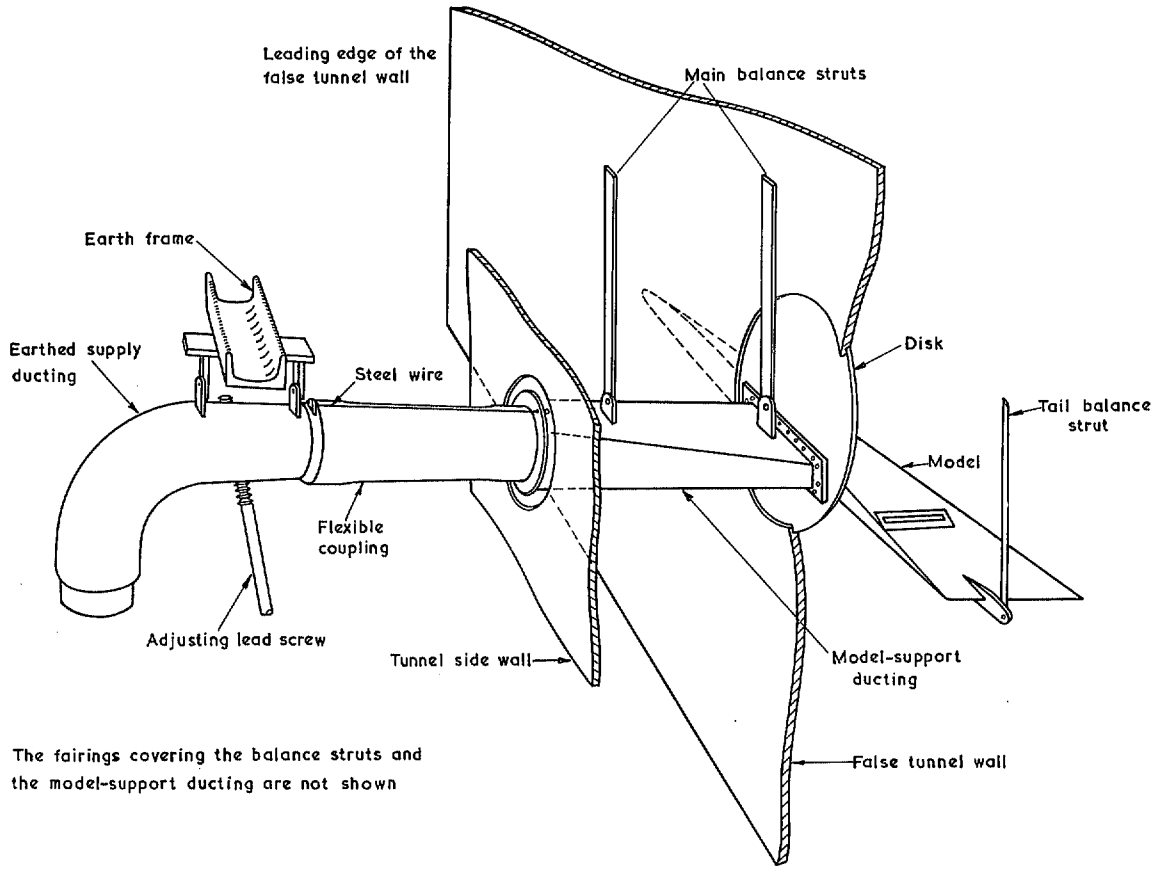

FIG. 3. The model-support system and the false tunnel wall.

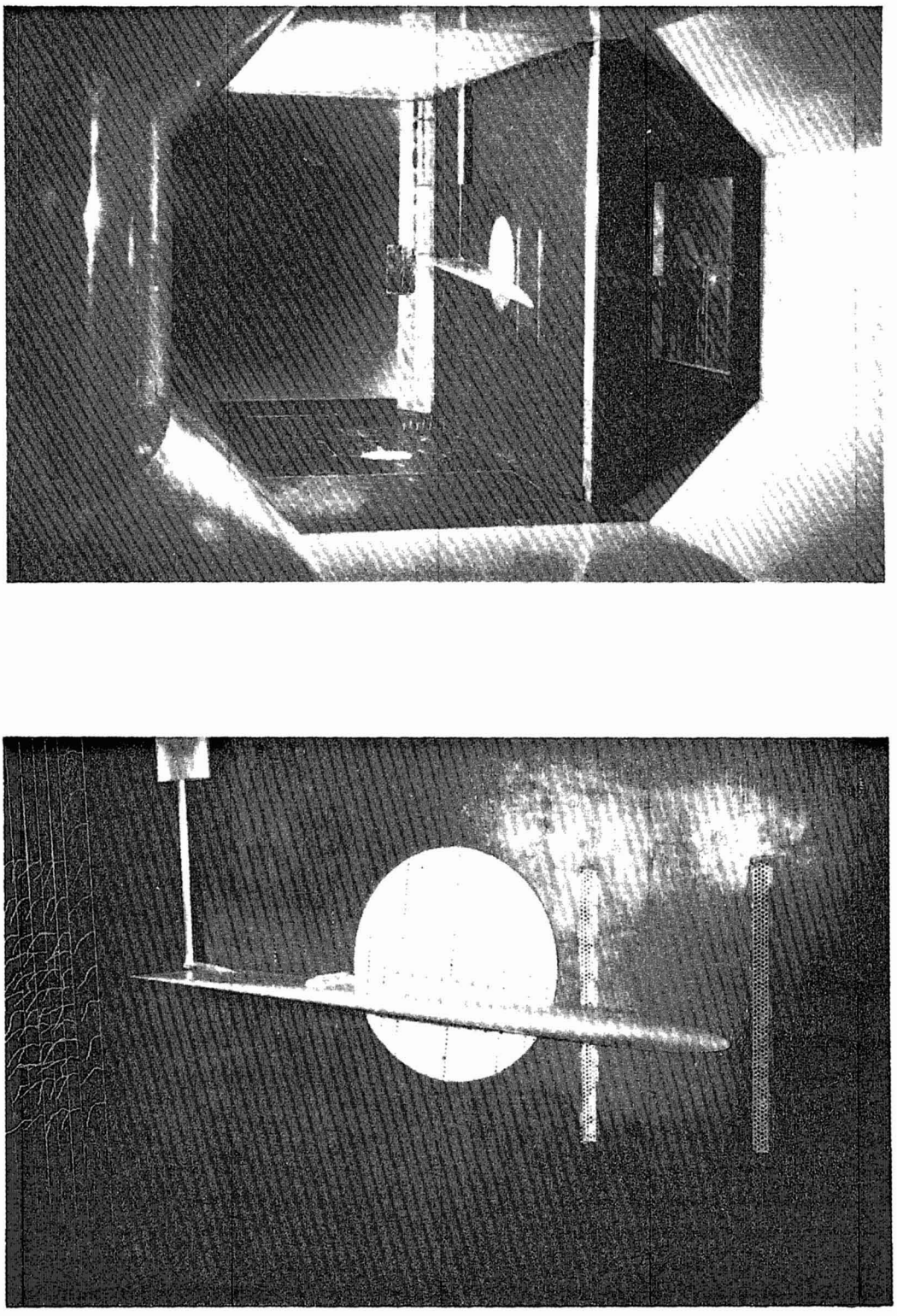

FIG. 4. The half model and the false tunnel wall.

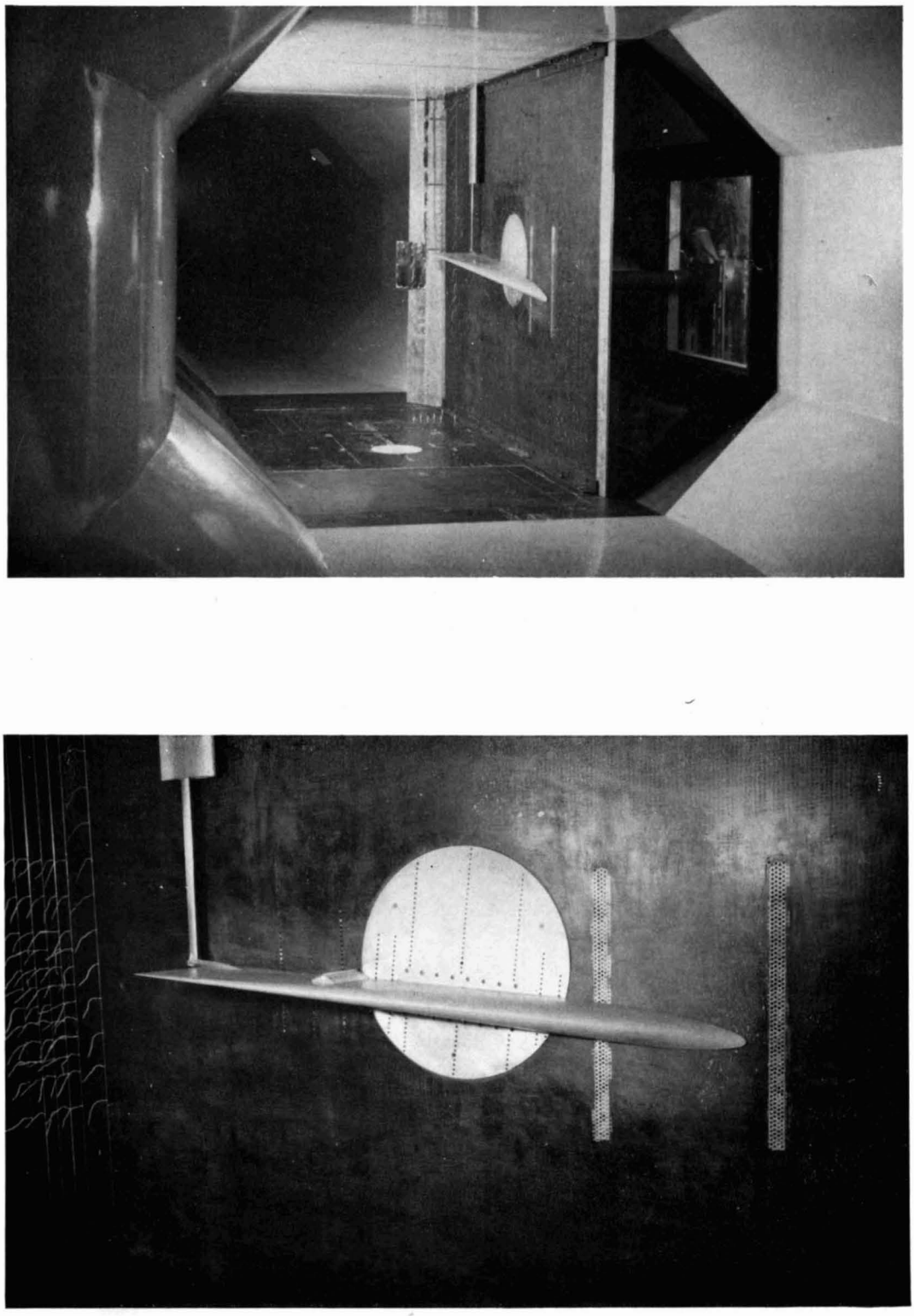

FIG. 4. The half model and the false tunnel wall.

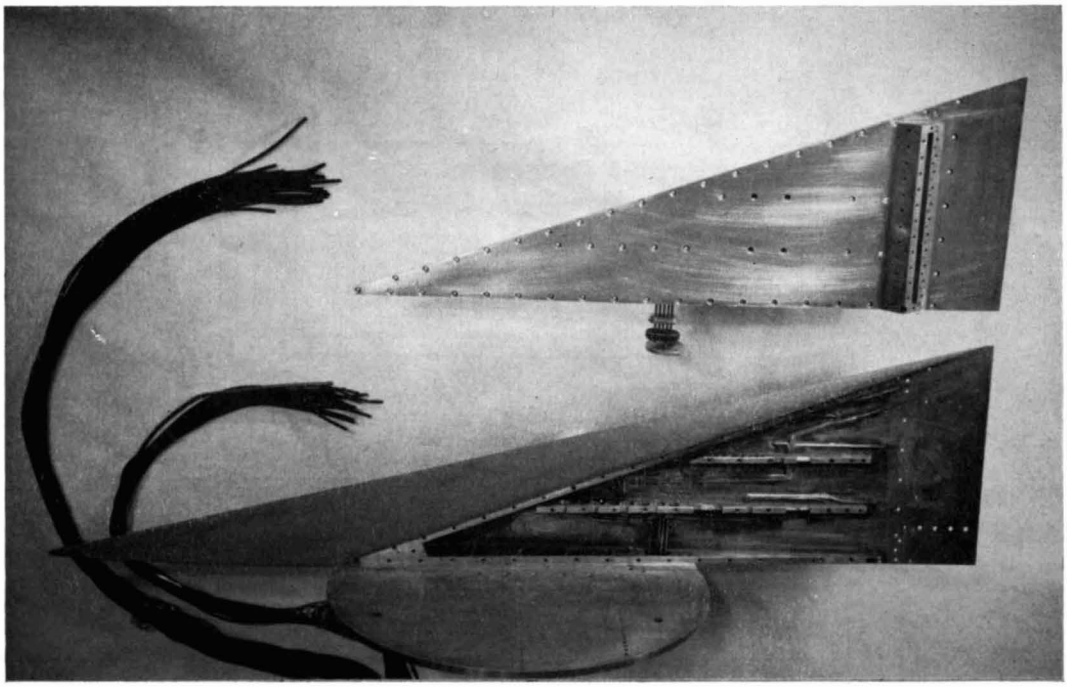

FIG. 5. Internal view of the half model.

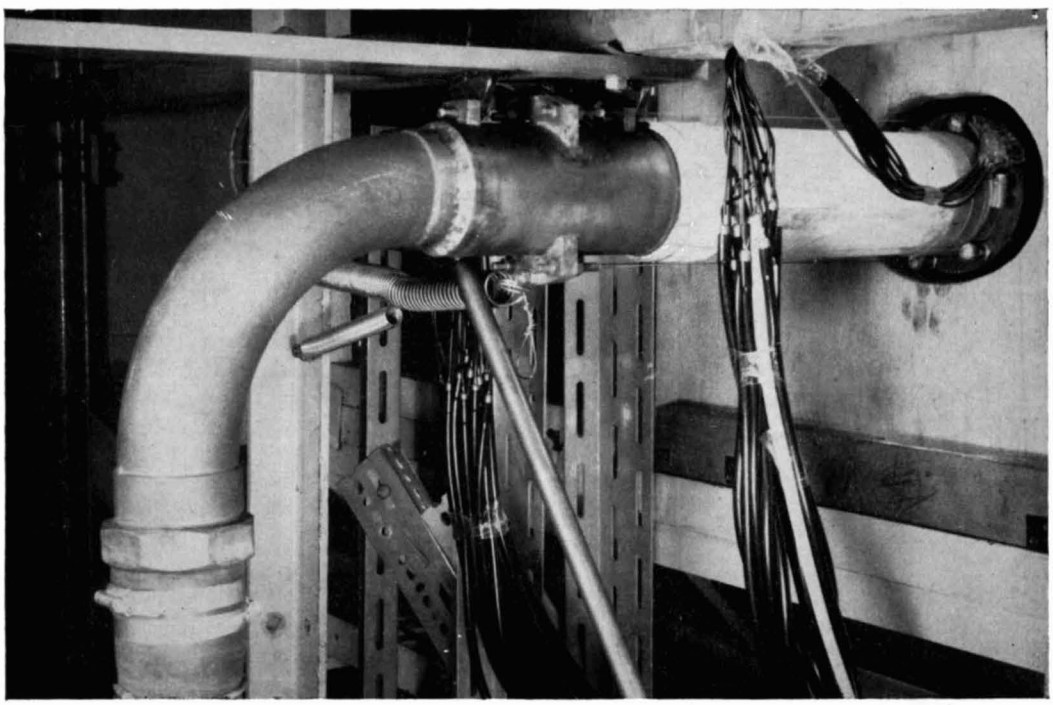

FIG. 6. The flexible coupling, air-bearing connector in position.

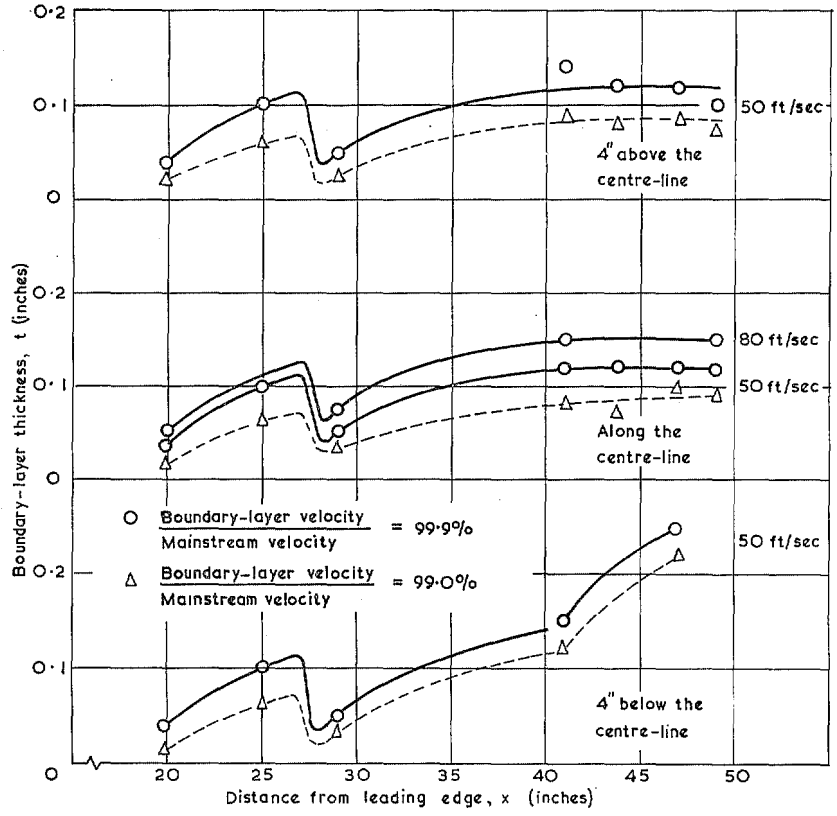

FIG. 9. Boundary-layer thickness on the false tunnel wall in the region of the model, for two tunnel velocities.

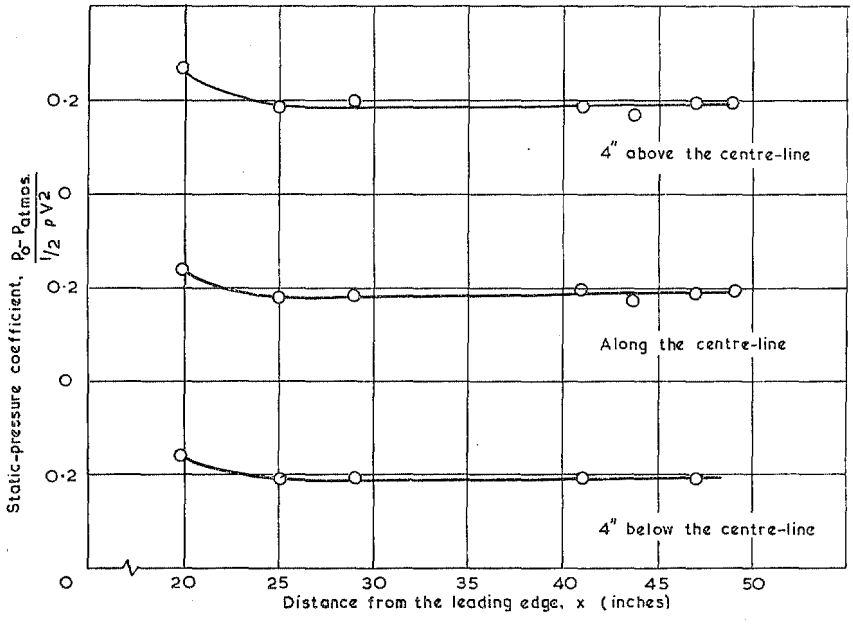

FIG. 10. Static-pressure coefficient on the false tunnel wall in the region of the model.

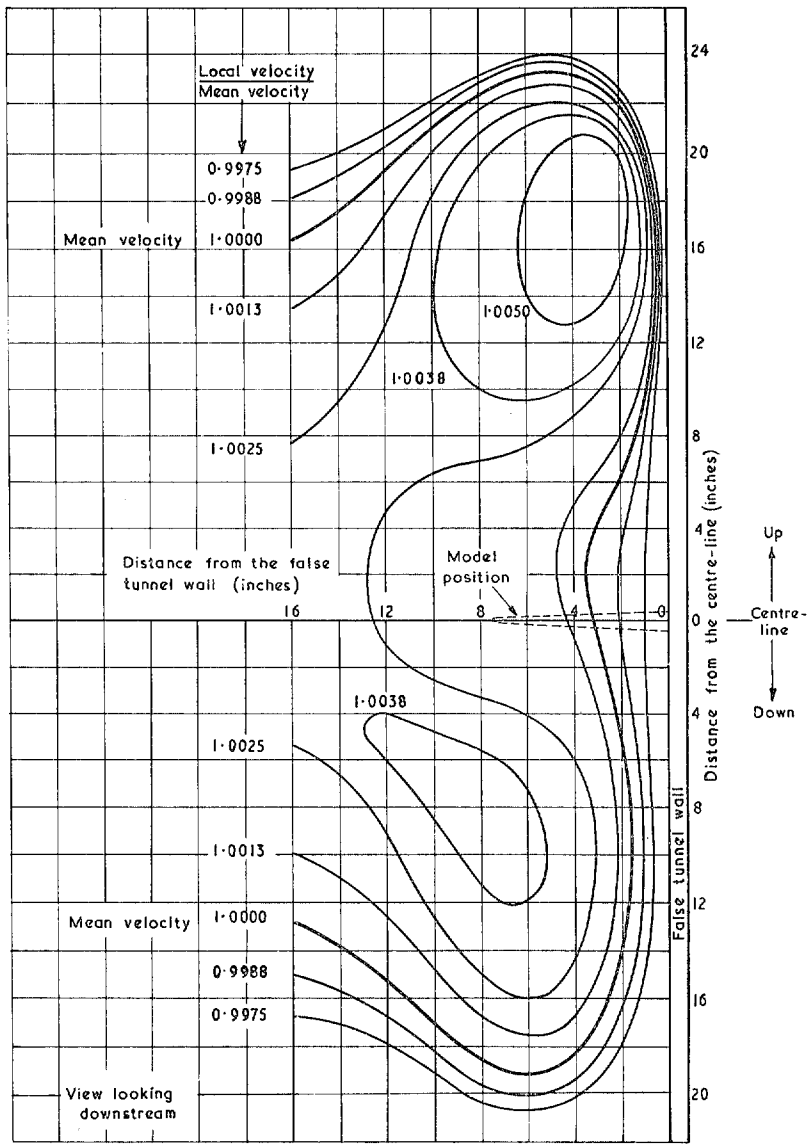

FIG. 11. Cross-sectional velocity profile of the tunnel working section. At $x_w = 20$ inches.

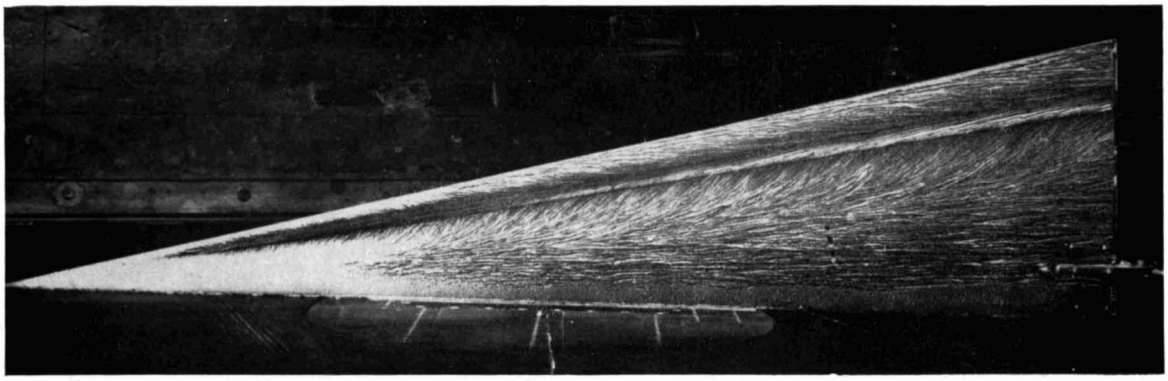

(a) No boundary-layer suction.

(b) Full boundary-layer suction.

FIGS. 12 a and b. China-clay flow patterns on the flat-plate delta to show the effect of the boundary-layer control on the false tunnel wall.

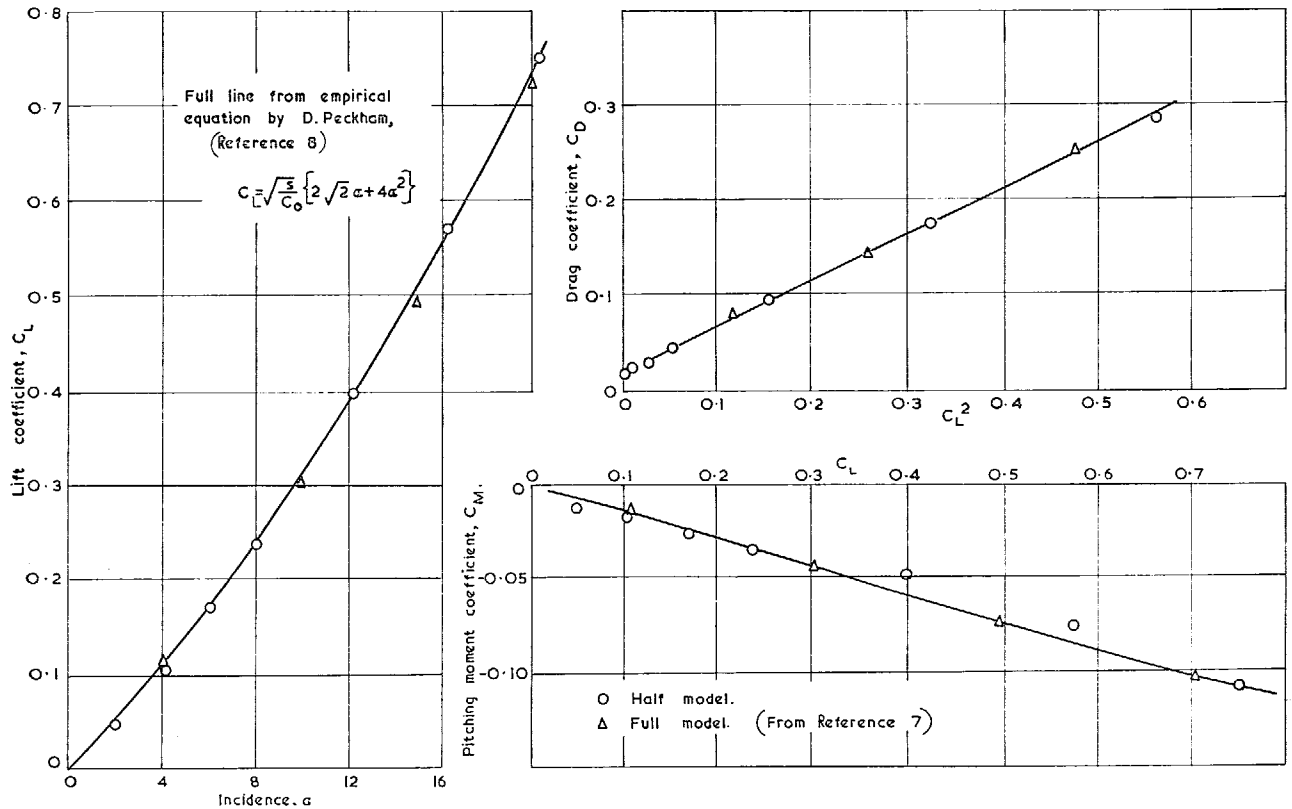

FIG. 13. Comparison of results from the half-model flat plate (sharp leading edge, and $A = 1$) with similar full-model tests.

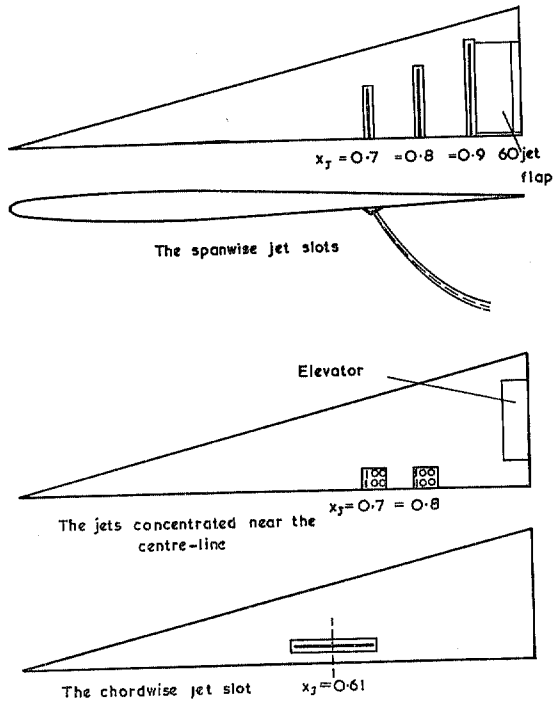

FIG. 14. Sketch of the various jet configurations tested.

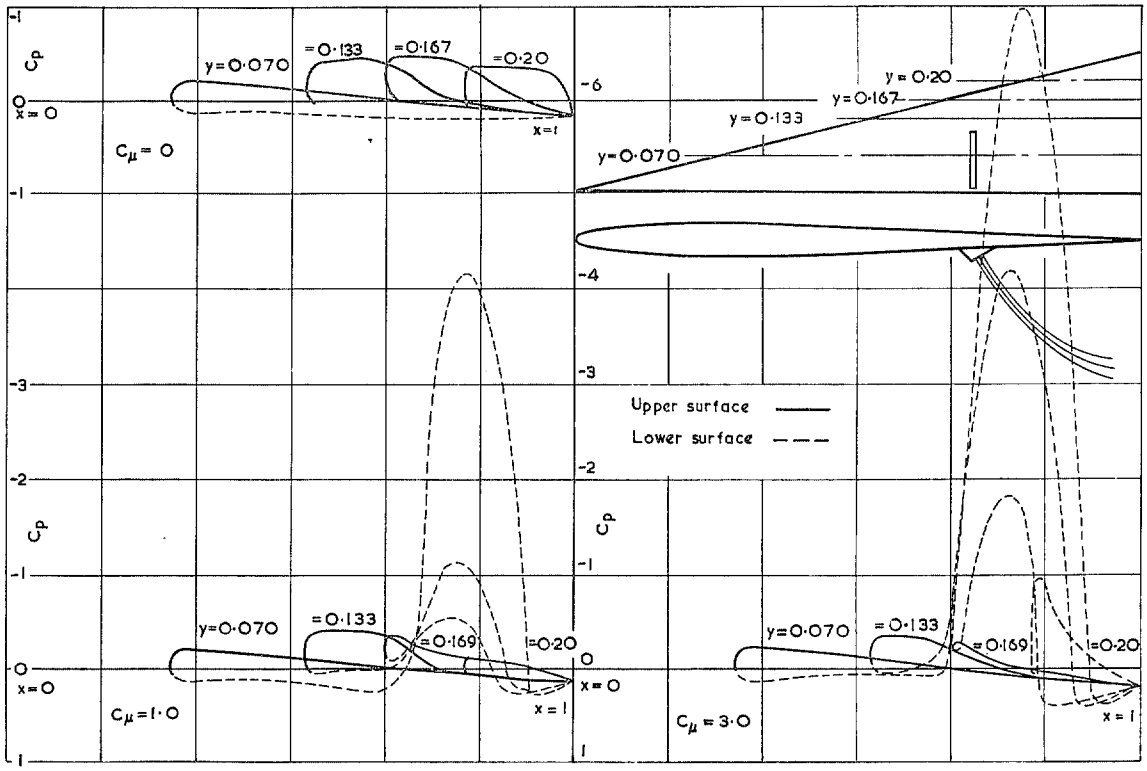

FIG. 15. Pressure coefficients plotted along four chordwise lines for the spanwise jet slot at $x_J = 0{\cdot}7$, for $C_\mu = 0$, 1 and 3; at incidence $\alpha = 8$ deg. $S_J/S = 0{\cdot}356$ per cent, $\alpha_J = 60$ deg, $R = 5{\cdot}2 \times 10^5$.

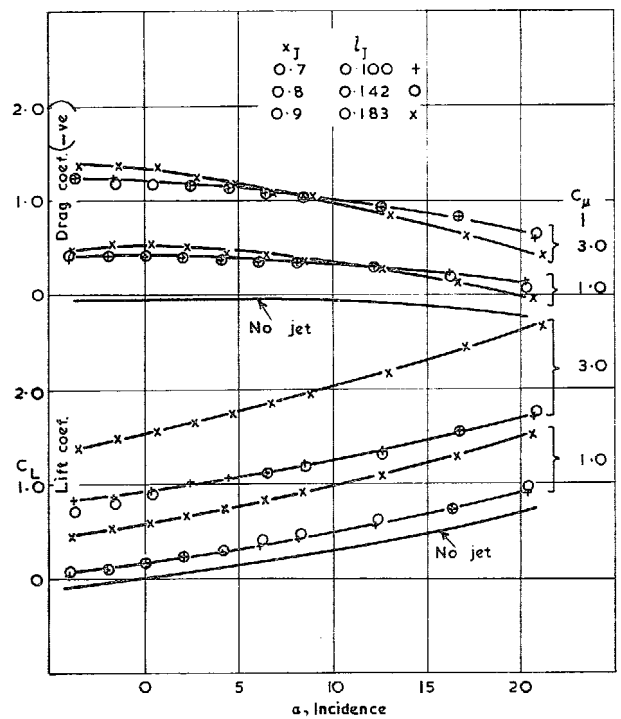

FIG. 16. Overall lift and drag coefficients for the spanwise jet slots at $x_J = 0{\cdot}7$, $0{\cdot}8$ and $0{\cdot}9$, for $C_\mu = 1{\cdot}0$ and $3{\cdot}0$. $S_J/S = 0{\cdot}356$ per cent, $\alpha_J = 60$ deg, $R = 5{\cdot}2 \times 10^5$.

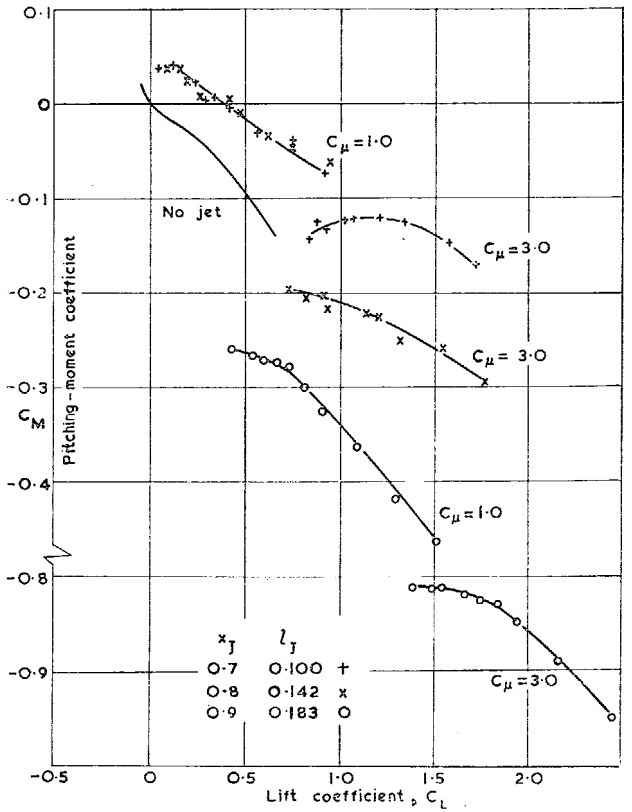

FIG. 17. Pitching-moment coefficients for the spanwise jet slots at $x_J = 0{\cdot}7$, $0{\cdot}8$ and $0{\cdot}9$. Incidence from -4 deg to 20 deg, for $C_\mu = 1{\cdot}0$ and $3{\cdot}0$. $S_J/S = 0{\cdot}356$ per cent, $\alpha_J = 60$ deg, $R = 5{\cdot}2 \times 10^5$.

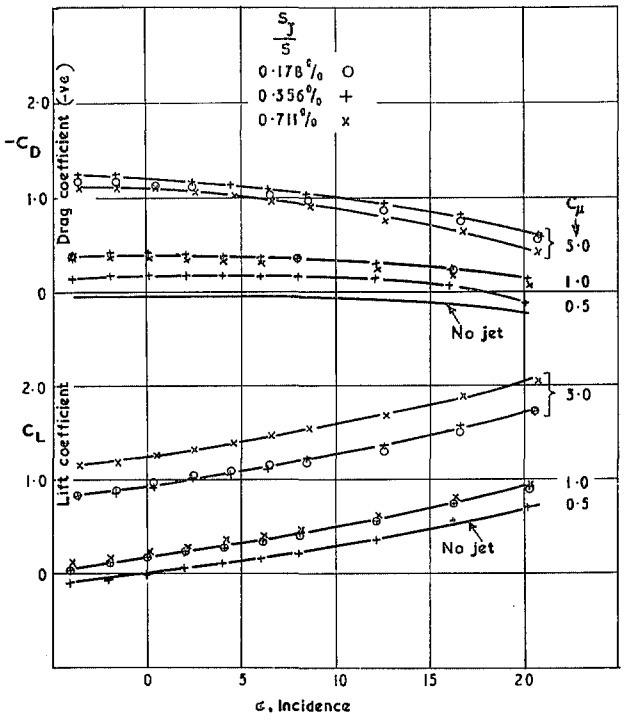

FIG. 18. Overall lift and drag coefficients for the spanwise jet slot at $x_J = 0{\cdot}7$ for various S_J/S ratios, and C_μ. $l_J = 0{\cdot}10$, $\alpha_J = 60$ deg, $R = 5{\cdot}2 \times 10^5$.

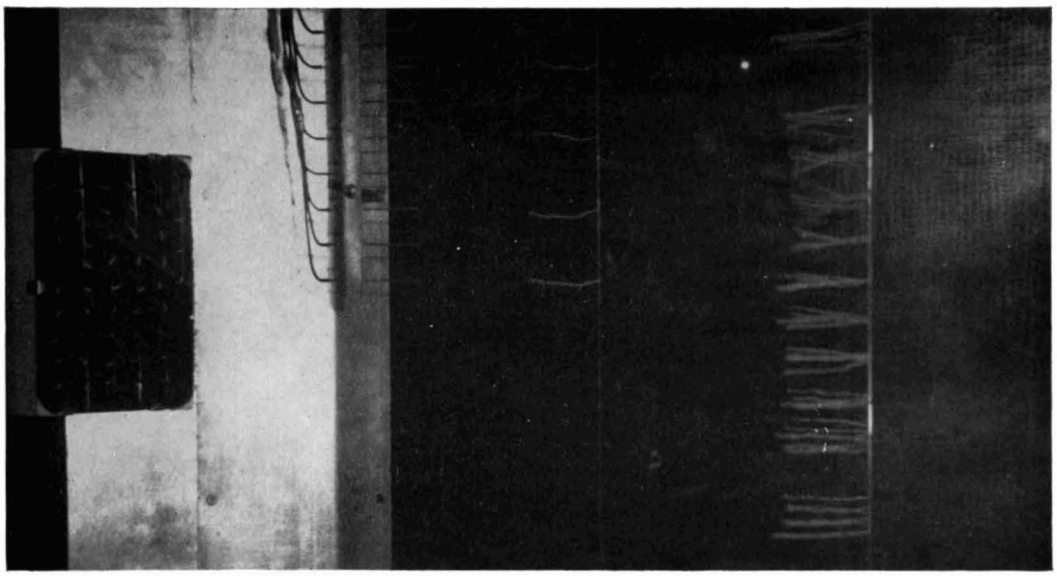

(a) The normal leading-edge vortex formed by the separation of the flow from the lower to the upper surface, for $\alpha = 12$ deg, $C_\mu = 0$.

(b) The reverse leading-edge vortex separating from the upper to the lower surface for $\alpha = 2$ deg, $C_\mu = 4{\cdot}0$.

The mirror is showing a view normal to the screen of tufts (one inch apart); *i.e.*, looking down the core of the vortex. The jet is at $x_J = 0{\cdot}7$, $\alpha_J = 60$ deg, $S_J/S = 0{\cdot}356$ per cent.

FIGS. 19 a and b. Flow visualization of the vortex, with wool tufts at $\frac{1}{3}$ C_0 behind the trailing edge.

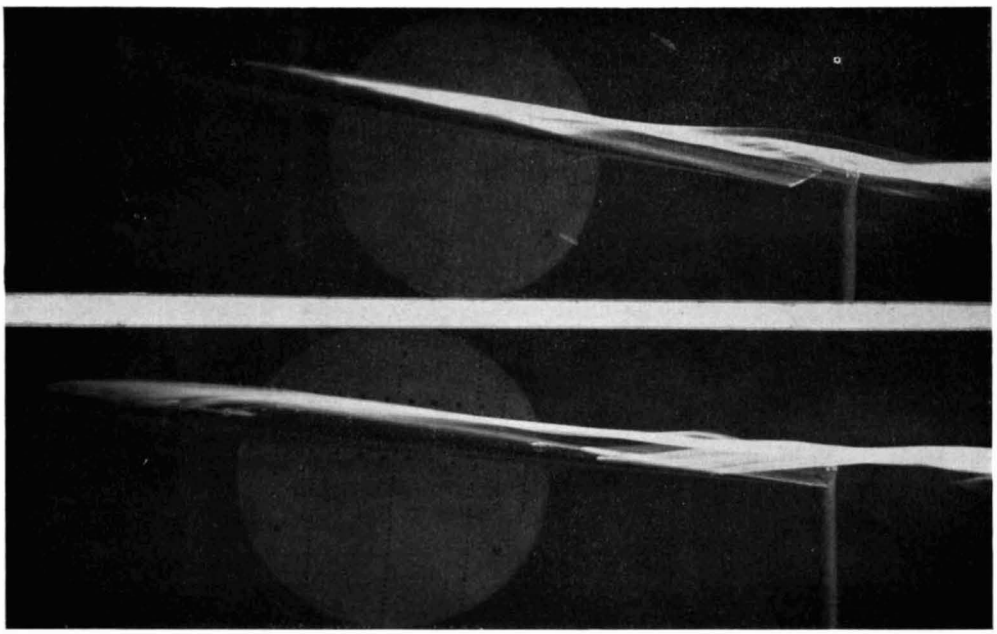

(a) No-jet-blowing condition of the leading-edge vortex.

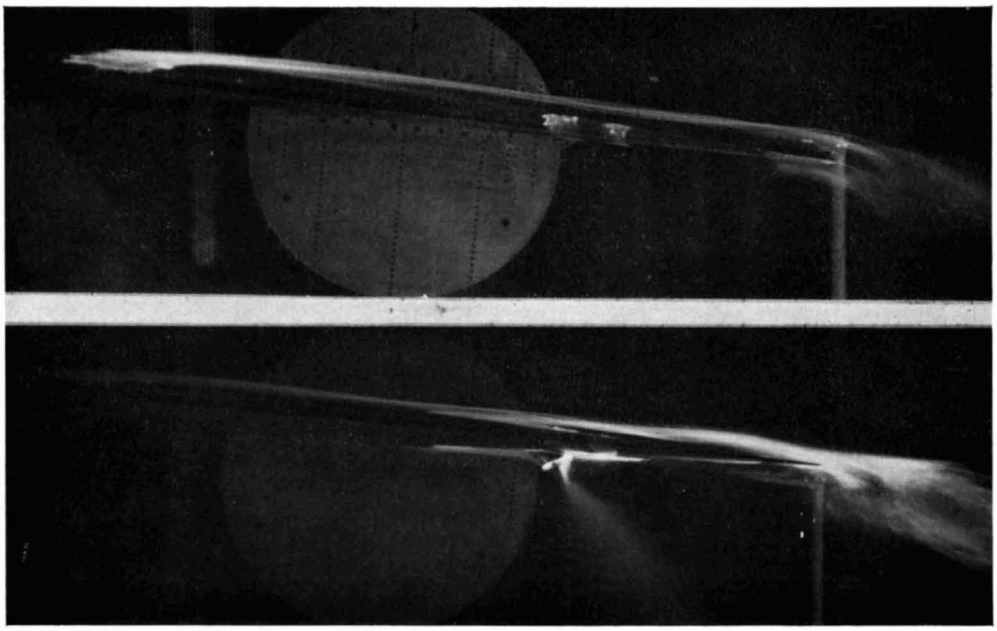

(b) Jet blowing, showing the flow from the upper to the lower surface and the breakdown of the original leading-edge vortex into the reverse vortex at the rear.

FIGS. 20 a and b. Titanic chloride flow visualization with the chordwise jet at $x_J = 0{\cdot}7$.

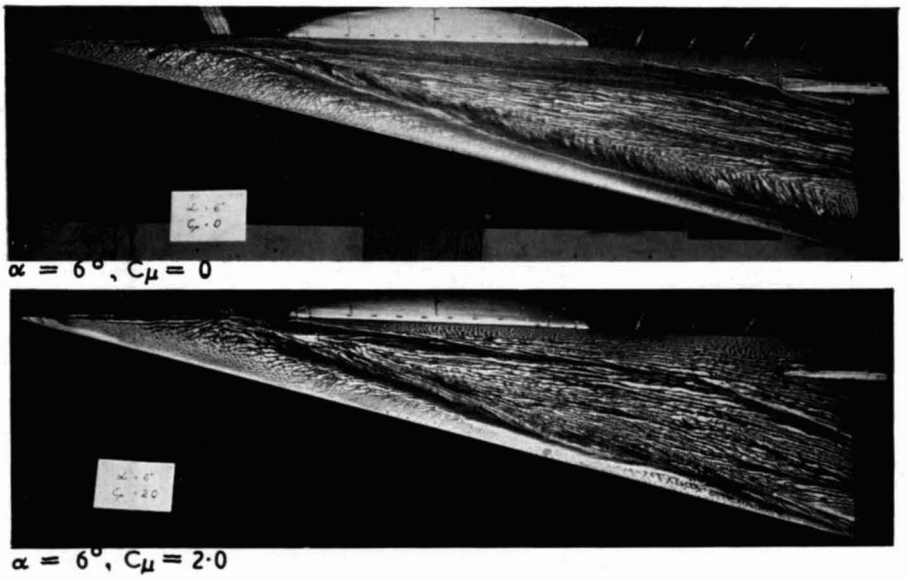

(a) Upper surface.

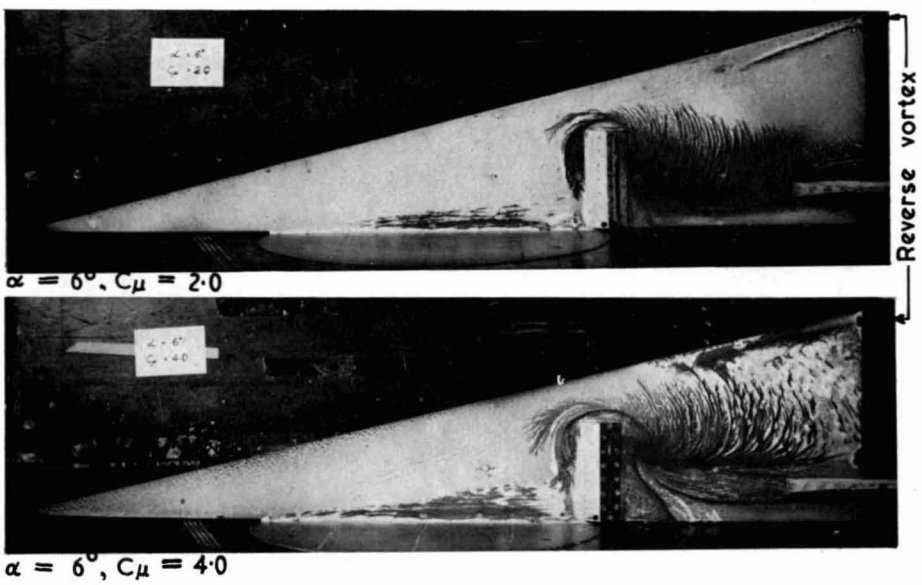

(b) Lower surface.

Showing the complete breakdown of the normal leading-edge vortex into the reverse leading-edge vortex, formed by the separation of the flow from the upper surface to the low-pressure area behind the jet on the lower surface.

FIGS. 21 a and b. China-clay flow patterns for the spanwise jet at $x_J = 0{\cdot}7$, $\alpha_J = 60$ deg, $S_J/S = 0{\cdot}356$ per cent.

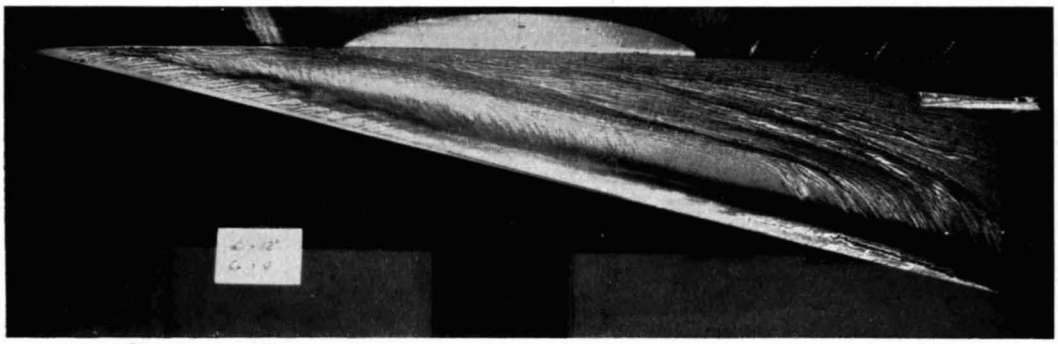

$\alpha = 12°, C_\mu = 0$

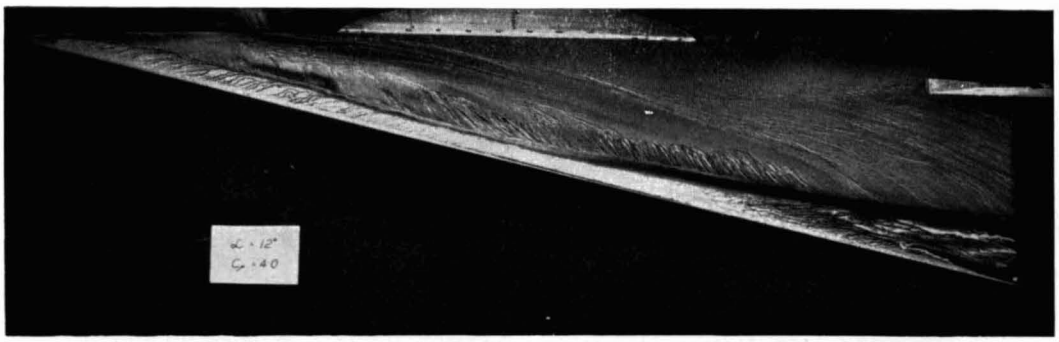

$\alpha = 12°, C_\mu = 4{\cdot}0$

(a) Upper surface.

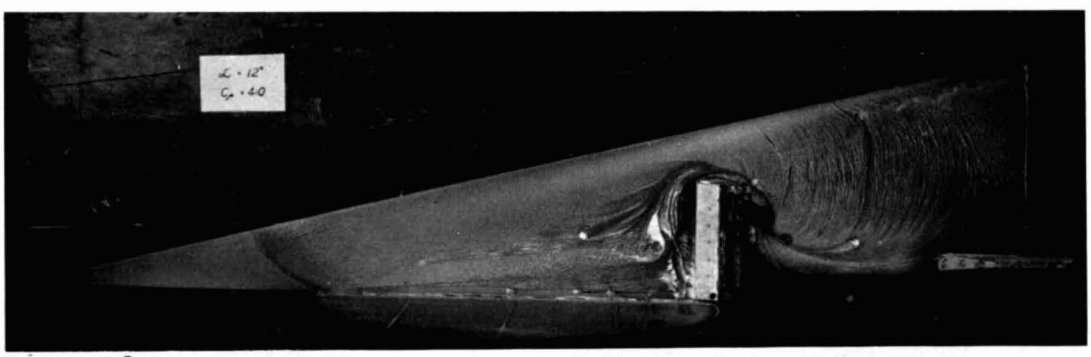

$\alpha = 12°, C_\mu = 4{\cdot}0$

(b) Lower surface.

Showing the distortion of the normal leading-edge vortex over the upper surface induced by the spanwise jet sheet.

FIGS. 22 a and b. China-clay flow patterns for the spanwise jet at $x_J = 0{\cdot}7$, $\alpha_J = 60$ deg, $S_J/S = 0{\cdot}356$ per cent.

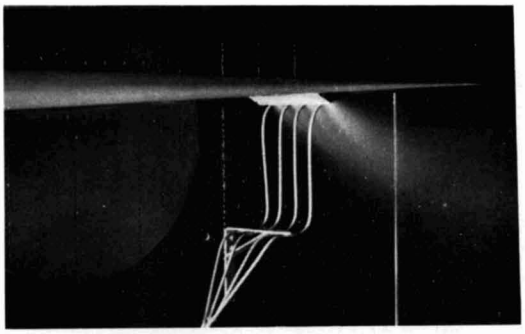

$C_\mu = 0{\cdot}5$

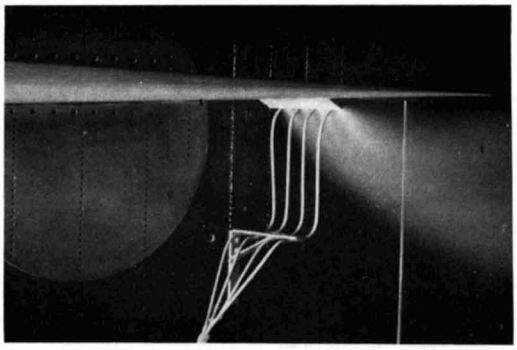

$C_\mu = 1{\cdot}0$

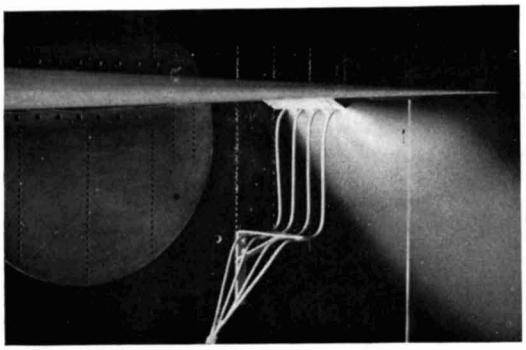

$C_\mu = 3{\cdot}0$

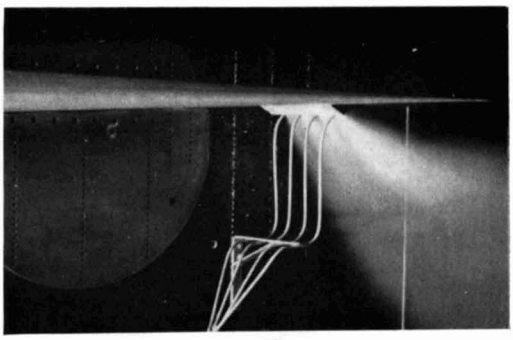

$C_\mu = 5{\cdot}0$

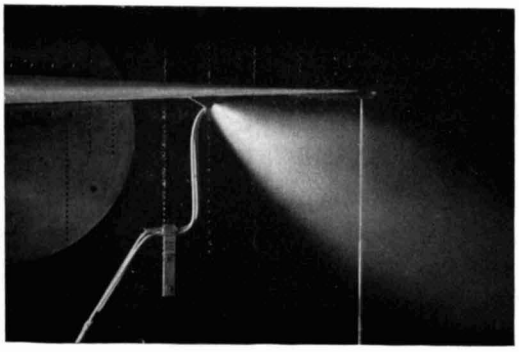

$C_\mu = 3{\cdot}0$

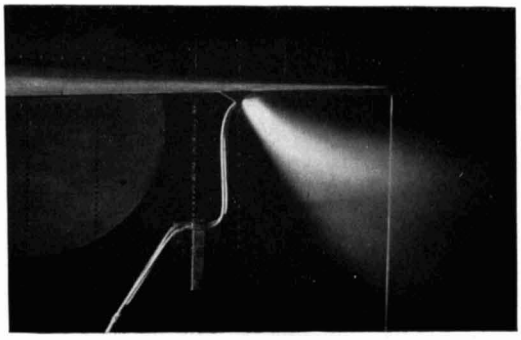

$C_\mu = 5{\cdot}0$

Showing the way in which the edge of the jet sheet is rolling up into a vortex.

FIG. 23. Water flow visualization of the spanwise jet at $x_J = 0{\cdot}8$, $\alpha_J = 60$ deg, $S_J/S = 0{\cdot}356$ per cent and $\alpha = 0$ deg.

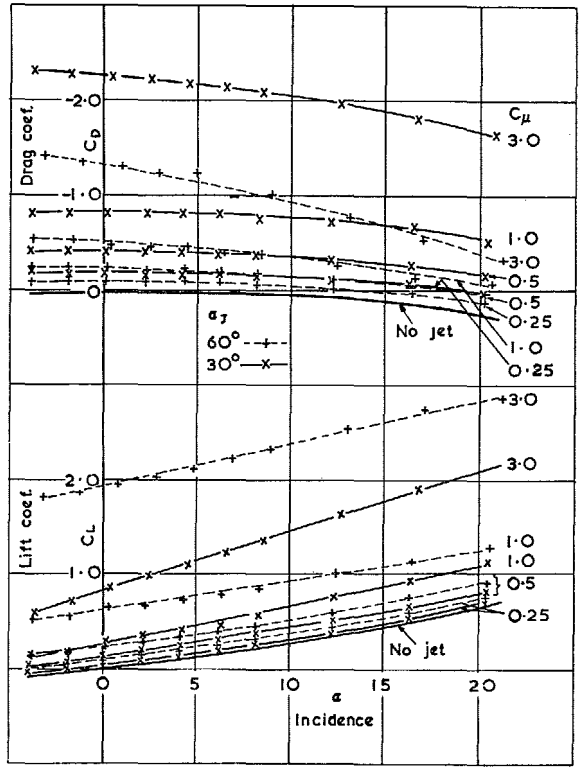

FIG. 24. Overall lift and drag coefficients for the jets grouped near the centre-line at $x_J = 0{\cdot}7$, $S_J/S = 0{\cdot}356$ per cent, $R = 5{\cdot}2 \times 10^5$.

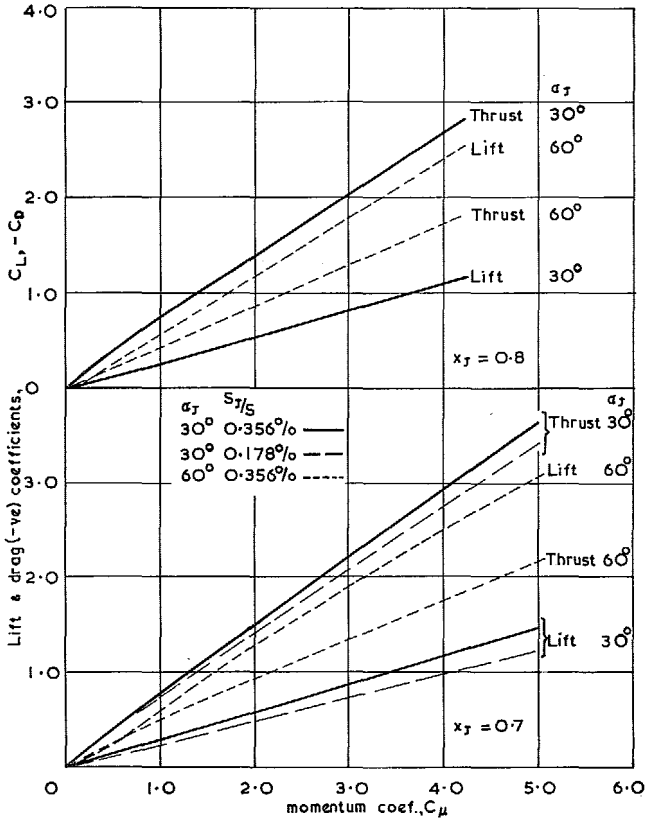

FIG. 25. Overall lift and drag coefficients for the jets grouped near the centre-line for $\alpha = 0$, at $x_J = 0{\cdot}7$ and $0{\cdot}8$. $R = 5{\cdot}2 \times 10^5$.

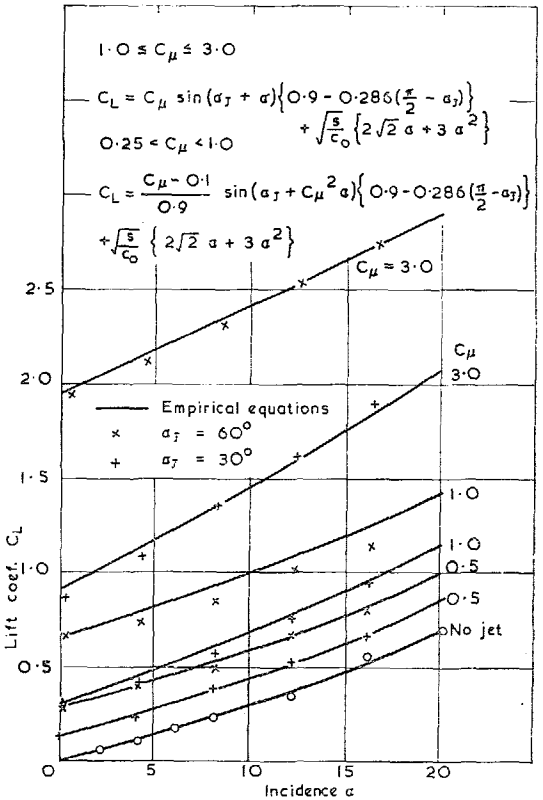

FIG. 26. Comparison of the empirical equations for lift coefficient with experimental results at $x_J = 0{\cdot}7$, $S_J/S = 0{\cdot}356$ per cent.

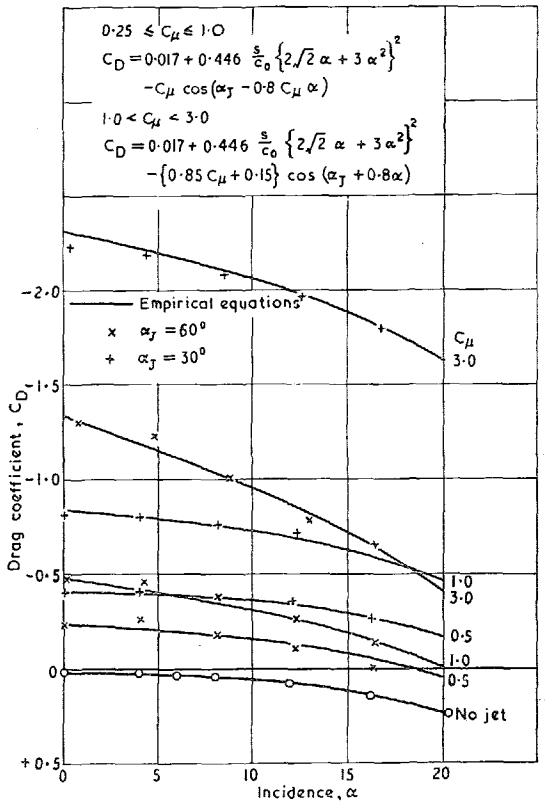

FIG. 27. Comparison of the empirical equations for drag coefficient with experimental results at $x_J = 0{\cdot}7$, $S_J/S = 0{\cdot}356$ per cent.

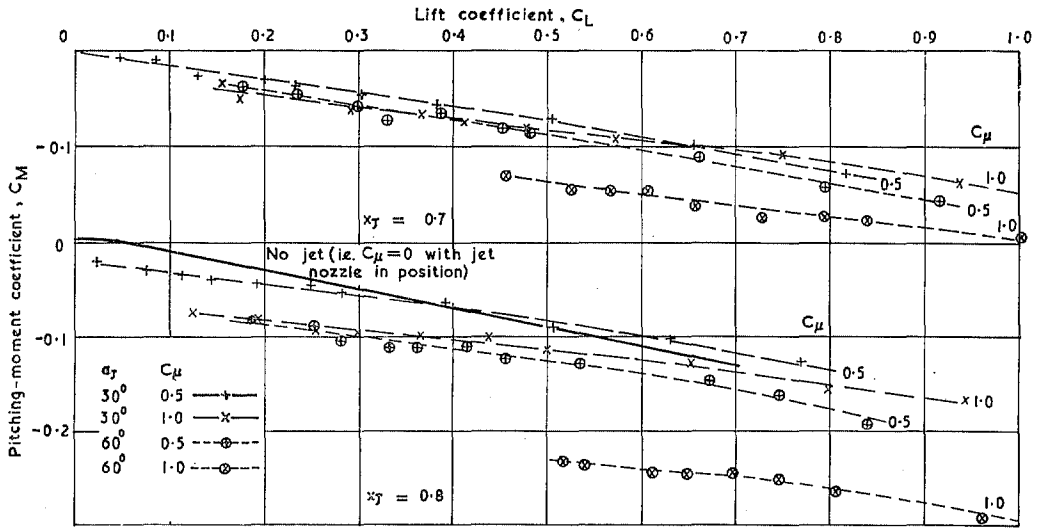

FIG. 28a. Overall pitching-moment coefficients for the jets grouped near the centre-line at $x_J = 0{\cdot}7$ and $0{\cdot}8$, $S_J/S = 0{\cdot}356$ per cent, $R = 5{\cdot}2 \times 10^5$.

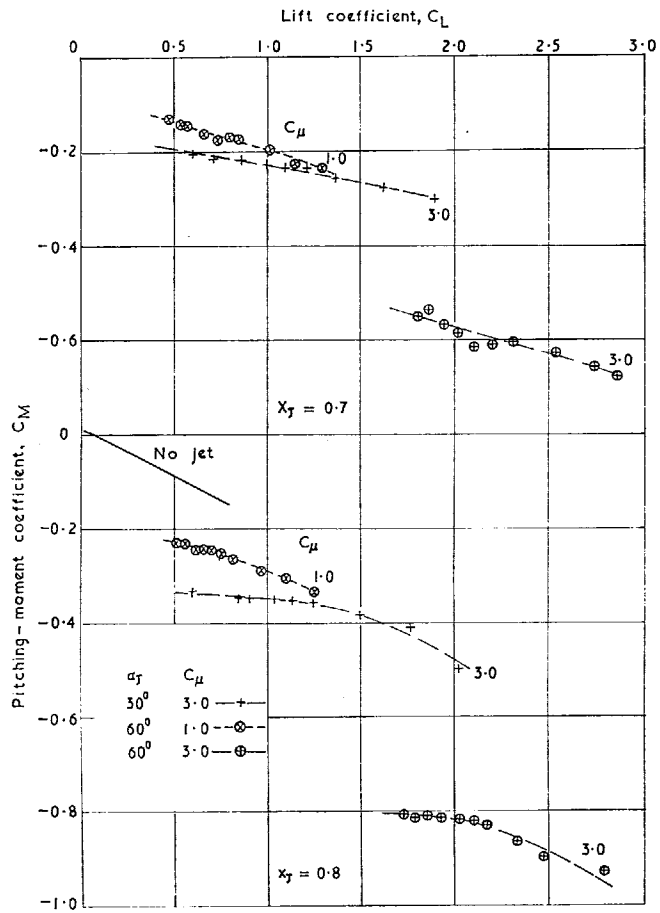

FIG. 28b. Overall pitching-moment coefficients for the jets grouped near the centre-line at $x_J = 0{\cdot}7$ and $0{\cdot}8$, $S_J/S = 0{\cdot}356$ per cent, $R = 5{\cdot}2 \times 10^5$.

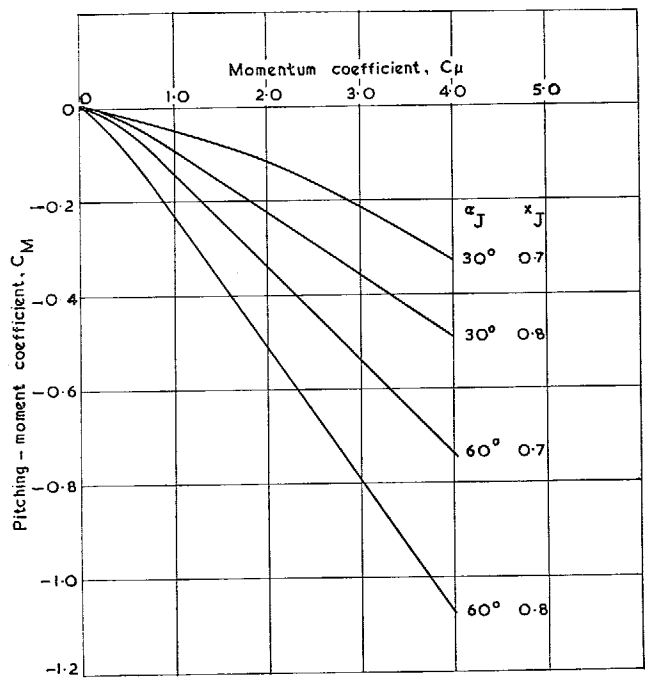

FIG. 29. Overall pitching-moment coefficients for the jets grouped near the centre-line for $\alpha = 0$ at $x_J = 0{\cdot}7$ and $0{\cdot}8$. $R = 5{\cdot}2 \times 10^5$.

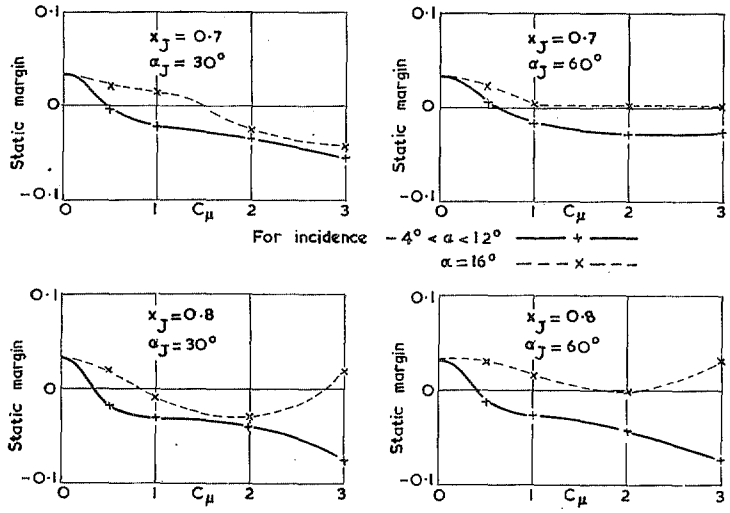

FIG. 30. Static margin based on C_0 and with the centre of gravity at $x = 0{\cdot}6$, as a function of C_μ, for the jets grouped near the centre-line.

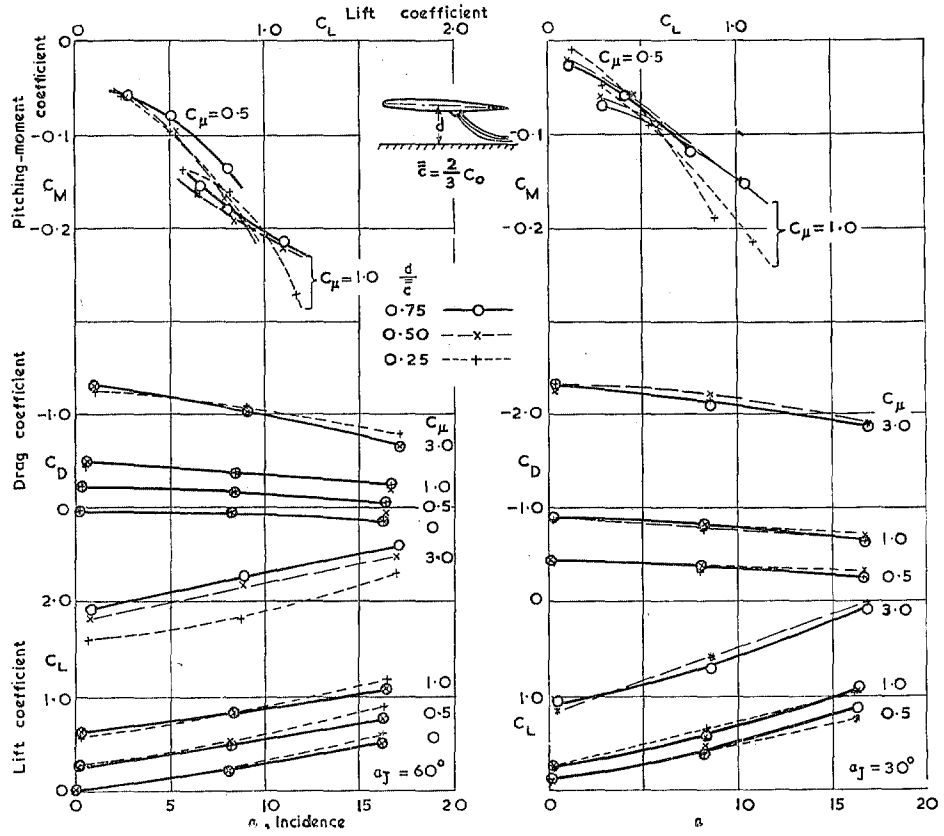

FIG. 31. Overall lift, drag and pitching-moment coefficients with ground interference, for the jets grouped near the centre-line. $x_J = 0{\cdot}7$, $S_J/S = 0{\cdot}356$ per cent, $R = 5{\cdot}2 \times 10^5$.

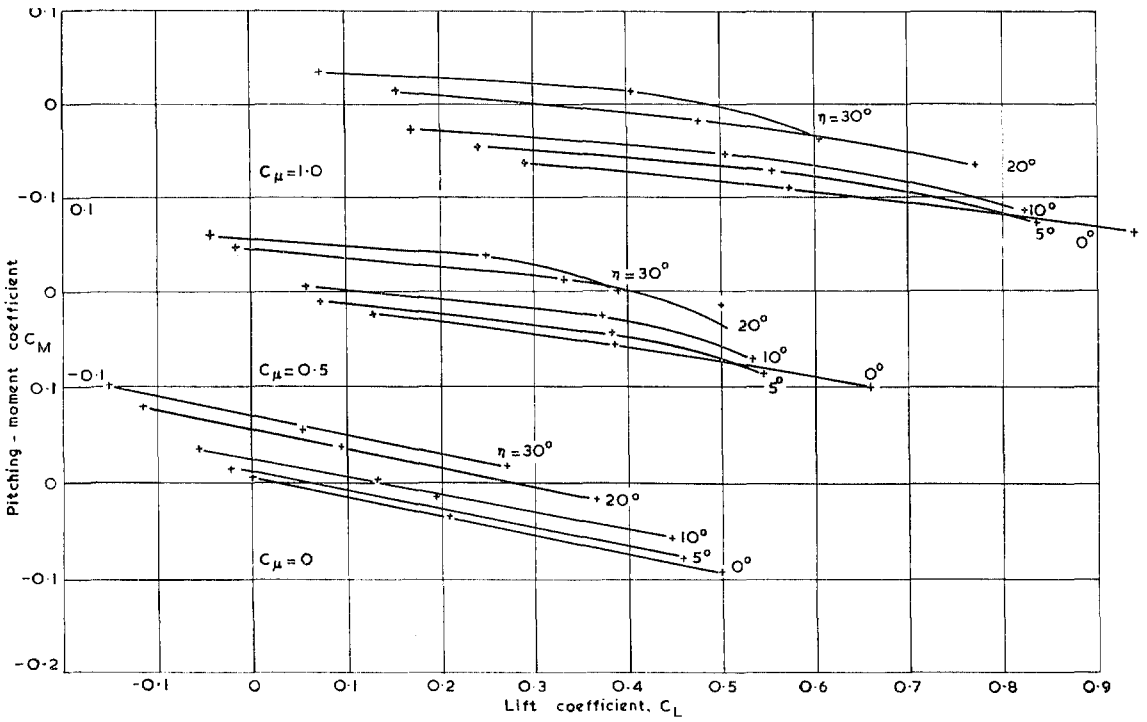

FIG. 32. Overall pitching-moment coefficient with an elevator, 60 per cent T.E. span, 0·05 C_0 chord, with the jets grouped near the centre-line at $x_J = 0{\cdot}7$, $\alpha_J = 30$ deg, $S/S_J = 0{\cdot}356$ per cent, $R = 5{\cdot}2 \times 10^5$.

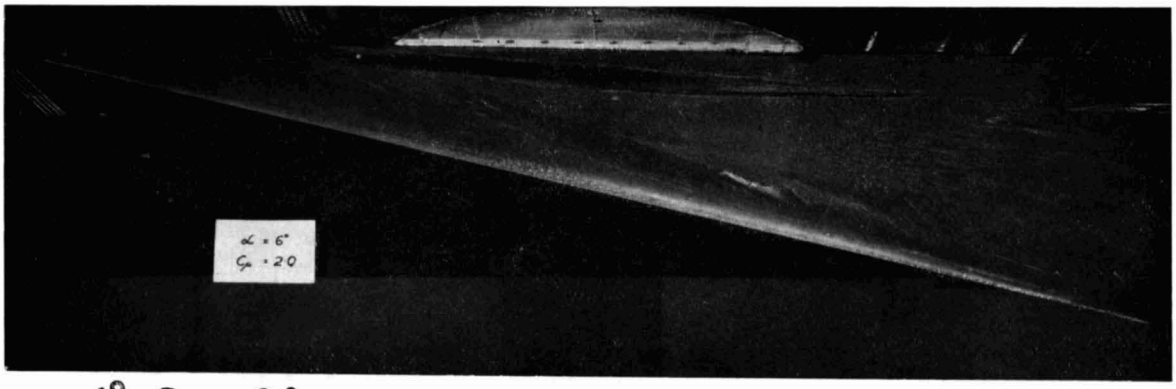

$\alpha = 6^{\circ}, C_{\mu} = 2{\cdot}0$

(a) Upper surface.

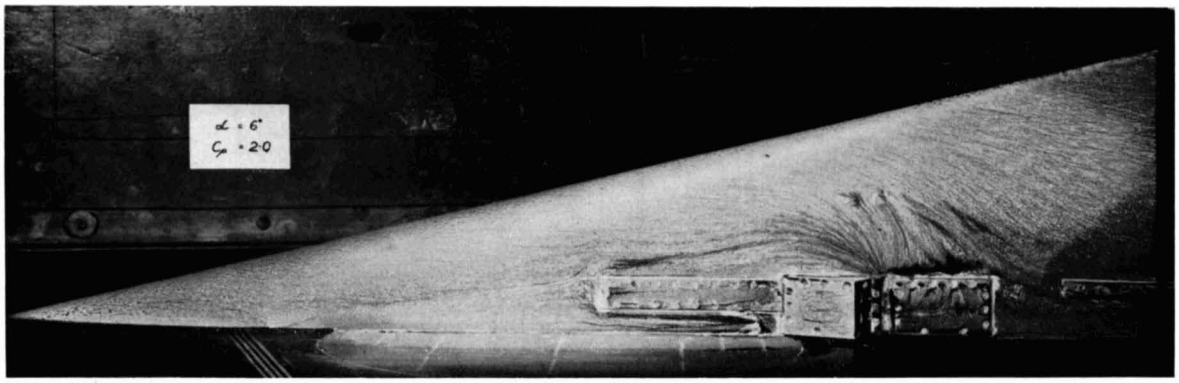

$\alpha = 6^{\circ}, C_{\mu} = 2{\cdot}0$

(b) Lower surface.

Showing the flow in the free-stream direction over the trailing edge, where a control surface can be effectively used.

FIGS. 33 a and b. China-clay flow patterns for the jets concentrated near the centre-line of the wing at $x_J = 0{\cdot}7$, $\alpha = 30$ deg, $S_J/S = 0{\cdot}356$ per cent.

(85435) Wt. 64/1857 K.5 11/62 Hw.

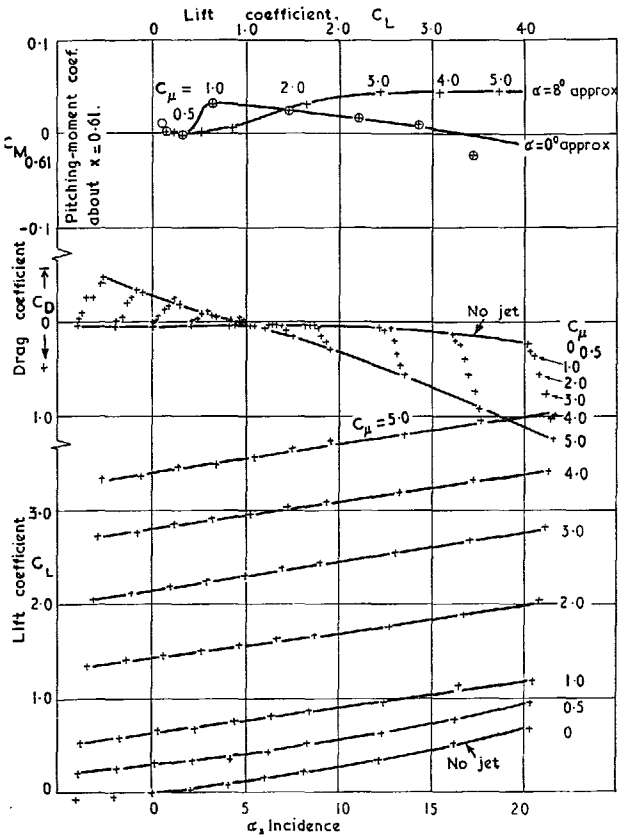

FIG. 34. Overall lift, drag and pitching-moment (about $x = 0{\cdot}61$) coefficients for the vertically directed chordwise jet at $x_J = 0{\cdot}61$.

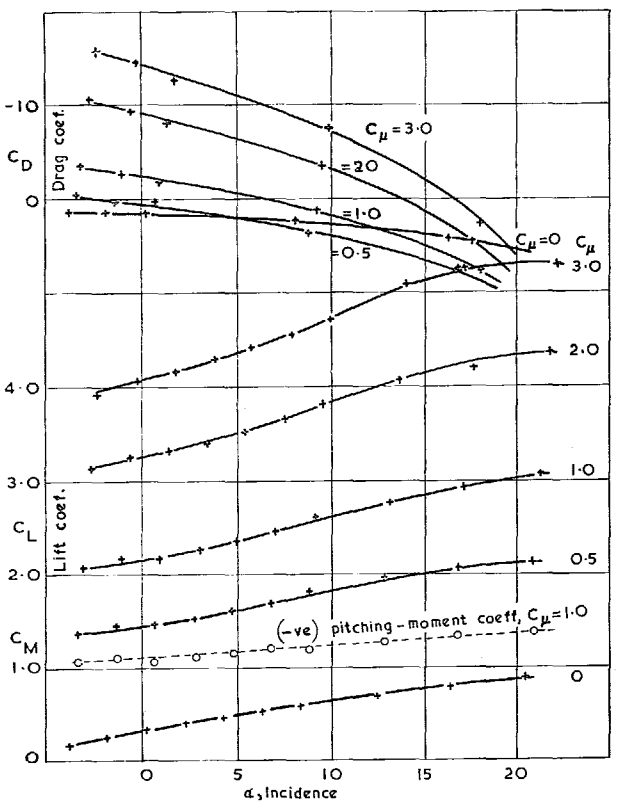

FIG. 35. Overall lift, drag and pitching-moment coefficients for the jet flap. $\alpha_J = 60$ deg, $R = 5{\cdot}2 \times 10^5$.

Publications of the Aeronautical Research Council

ANNUAL TECHNICAL REPORTS OF THE AERONAUTICAL RESEARCH COUNCIL (BOUND VOLUMES)

1942 Vol. I. Aero and Hydrodynamics, Aerofoils, Airscrews, Engines. 75*s.* (post 2*s.* 9*d.*)
Vol. II. Noise, Parachutes, Stability and Control, Structures, Vibration, Wind Tunnels. 47*s.* 6*d.* (post 2*s.* 3*d.*)

1943 Vol. I. Aerodynamics, Aerofoils, Airscrews. 80*s.* (post 2*s.* 6*d.*)
Vol. II. Engines, Flutter, Materials, Parachutes, Performance, Stability and Control, Structures. 90*s.* (post 2*s.* 9*d.*)

1944 Vol. I. Aero and Hydrodynamics, Aerofoils, Aircraft, Airscrews, Controls. 84*s.* (post 3*s.*)
Vol. II. Flutter and Vibration, Materials, Miscellaneous, Navigation, Parachutes, Performance, Plates and Panels, Stability, Structures, Test Equipment, Wind Tunnels. 84*s.* (post 3*s.*)

1945 Vol. I. Aero and Hydrodynamics, Aerofoils. 130*s.* (post 3*s.* 6*d.*)
Vol. II. Aircraft, Airscrews, Controls. 130*s.* (post 3*s.* 6*d.*)
Vol. III. Flutter and Vibration, Instruments, Miscellaneous, Parachutes, Plates and Panels, Propulsion. 130*s.* (post 3*s.* 3*d.*)
Vol. IV. Stability, Structures, Wind Tunnels, Wind Tunnel Technique. 130*s.* (post 3*s.* 3*d.*)

1946 Vol. I. Accidents, Aerodynamics, Aerofoils and Hydrofoils. 168*s.* (post 3*s.* 9*d.*)
Vol. II. Airscrews, Cabin Cooling, Chemical Hazards, Controls, Flames, Flutter, Helicopters, Instruments and Instrumentation, Interference, Jets, Miscellaneous, Parachutes. 168*s.* (post 3*s.* 3*d.*)
Vol. III. Performance, Propulsion, Seaplanes, Stability, Structures, Wind Tunnels. 168*s.* (post 3*s.* 6*d.*)

1947 Vol. I. Aerodynamics, Aerofoils, Aircraft. 168*s.* (post 3*s.* 9*d.*)
Vol. II. Airscrews and Rotors, Controls, Flutter, Materials, Miscellaneous, Parachutes, Propulsion, Seaplanes, Stability, Structures, Take-off and Landing. 168*s.* (post 3*s.* 9*d.*)

1948 Vol. I. Aerodynamics, Aerofoils, Aircraft, Airscrews, Controls, Flutter and Vibration, Helicopters, Instruments, Propulsion, Seaplane, Stability, Structures, Wind Tunnels. 130*s.* (post 3*s.* 3*d.*)
Vol. II. Aerodynamics, Aerofoils, Aircraft, Airscrews, Controls, Flutter and Vibration, Helicopters, Instruments, Propulsion, Seaplane, Stability, Structures, Wind Tunnels. 110*s.* (post 3*s.* 3*d.*)

Special Volumes

Vol. I. Aero and Hydrodynamics, Aerofoils, Controls, Flutter, Kites, Parachutes, Performance, Propulsion, Stability. 126*s.* (post 3*s.*)
Vol. II. Aero and Hydrodynamics, Aerofoils, Airscrews, Controls, Flutter, Materials, Miscellaneous, Parachutes, Propulsion, Stability, Structures. 147*s.* (post 3*s.*)
Vol. III. Aero and Hydrodynamics, Aerofoils, Airscrews, Controls, Flutter, Kites, Miscellaneous, Parachutes, Propulsion, Seaplanes, Stability, Structures, Test Equipment. 189*s.* (post 3*s.* 9*d.*)

Reviews of the Aeronautical Research Council

1939–48 3*s.* (post 6*d.*) 1949–54 5*s.* (post 5*d.*)

Index to all Reports and Memoranda published in the Annual Technical Reports

1909–1947 R. & M. 2600 (out of print)

Indexes to the Reports and Memoranda of the Aeronautical Research Council

Between Nos. 2351–2449	R. & M. No. 2450	2*s.* (post 3*d.*)
Between Nos. 2451–2549	R. & M. No. 2550	2*s.* 6*d.* (post 3*d.*)
Between Nos. 2551–2649	R. & M. No. 2650	2*s.* 6*d.* (post 3*d.*)
Between Nos. 2651–2749	R. & M. No. 2750	2*s.* 6*d.* (post 3*d.*)
Between Nos. 2751–2849	R. & M. No. 2850	2*s.* 6*d.* (post 3*d.*)
Between Nos. 2851–2949	R. & M. No. 2950	3*s.* (post 3*d.*)
Between Nos. 2951–3049	R. & M. No. 3050	3*s.* 6*d.* (post 3*d.*)
Between Nos. 3051–3149	R. & M. No. 3150	3*s.* 6*d.* (post 3*d.*)

HER MAJESTY'S STATIONERY OFFICE

from the addresses overleaf

Printed and published by
HER MAJESTY'S STATIONERY OFFICE

To be purchased from
York House, Kingsway, London W.C.2
423 Oxford Street, London W.1
13A Castle Street, Edinburgh 2
109 St. Mary Street, Cardiff
39 King Street, Manchester 2
50 Fairfax Street, Bristol 1
35 Smallbrook, Ringway, Birmingham 5
80 Chichester Street, Belfast 1
or through any bookseller

Printed in England

S.O. Code No. 23-3288